INSTITUTO POLITÉCNICO DE BRAGANÇA
Escola Superior de Tecnologia e Gestão

UNIVERSIDADE TECNOLÓGICA FEDERAL DO PARANÁ

Power interface for grid-connected pico-hydro systems using PV inverters

Leonardo Candido da Silva

Thesis presented in the School of Technology and Management of the Polytechnic Institute of Bragança to fulfill the requirements of a Master of Science Degree in Industrial Engineering (Electrical Engineering branch).

Supervised by:

Prof. Dr. Américo Vicente Teixeira Leite

Prof. Dr. Ângela Paula Barbosa de Silva Ferreira

Prof. Dr. Luiz Francisco Sanches Buzachero

This work does not include the appointments and suggestions of the Juri

Bragança

2018-2019

INSTITUTO POLITÉCNICO DE BRAGANÇA Escola Superior de Tecnologia e Gestão

UTFPR
UNIVERSIDADE TECNOLÓGICA FEDERAL DO PARANÁ

Power interface for grid-connected pico-hydro systems using PV inverters

Leonardo Candido da Silva

Thesis presented in the School of Technology and Management of the Polytechnic Institute of Bragança to fulfill the requirements of a Master of Science Degree in Industrial Engineering (Electrical Engineering branch).

Supervised by:

Prof. Dr. Américo Vicente Teixeira Leite

Prof. Dr. Ângela Paula Barbosa de Silva Ferreira

Prof. Dr. Luiz Francisco Sanches Buzachero

Bragança

2018-2019

Acknowledgments

Firstly, I would like to thank all my relatives who have encouraged and cheered for me. I would like to express my most profound gratitude to Moadir, my father, Caroline, my sister and Franciele, my mother, who, even though, they were unwilling, they have supported my coming to Portugal. Without them, it would have been impossible. Despite the distance, they have managed to encourage and cheer me on.

I would like to thank my advisers Prof. Dr. Américo Vicente Leite and Prof. Dr. Ângela Paula Ferreira for their support, document reviews, criticisms, discussions and suggestions, contributing directly to the achieved results. Thanks to them, I was able to mature throughout this process. I would also like to acknowledge Prof. Batista for his assistance and help throughout this year.

I would like to thank my friends with whom I shared an apartment for a year in Bragança: Lucas Azevedo, Luis Guilherme, and Matheus Montanini. Without them, this year would not have been the same, with them, I have shared dreams, stories, happiness, and unluckiness in both good and bad moments that I will never forget.

Special thanks to all my new friends and colleagues I've made in Bragança, as well as those scattered around the world.

Finally, I would also like to acknowledge people not mentioned here who, whether directly or indirectly, contributed to the writing of this document.

Abstract

The electrical energy is a contemporaneous paradigm, the demand for electrical energy is ever-growing, and so is the energy supply; By bringing the energy production closer to the end-users, either in urban centers or people in remote areas have a chance to exploit renewable energy resources to produce electrical energy, and become self-sufficient. Hydropower has since long been a reliable power source, as well as being the most cost-effective. Although, it has its issues, e.g., its synchronization to the utility grid depends on the continuous operation mode of the generator.

Commercially available low-power inverters, up to 1.5 kW, are designed to be applied in either solar power generation, or wind power generation. These inverters were not designed to be used with hydropower generation. This work evaluates two current-controlled power interface solutions, boost and Ćuk converters, to make a hydropower generator and a commercial photovoltaic inverter compatible.

The models, simulations and tests of the proposed power structures along with a commercial photovoltaic inverter emulation are made with Matlab® Simulink®, facilitating the evaluation of the power structure and its controller in a discrete-time domain in a Simulation-in-the-Loop environment, as well as, an implementation using a Real-Time controller board from dSPACE interfacing between the power structure and the controller built-in Simulink® in a Hardware-in-the-Loop test platform with Commercial Phtovoltaic Inverter (CPVI), which allows for rapid prototyping, data acquisition and processing and experimental validation of the proposed solutions.

Keywords: Cuk Converter, Boost Converter, Power Interface, pico-hydro, PV inverters;

Contents

List of Tables

List of Figures

Acronyms

CCBC	Current-Controlled Boost Converter
CCCC	Current-Controlled Ćuk Converter
CPVI	Commercial Phtovoltaic Inverter
CVSI	Commercial Voltage Source Inverter
DC	Direct Current
DG	Distributed Generation
ESR	Equivalent Series Resistance
HIL	Hardware-in-the-Loop
IGBT	Insulated-gate Bipolar Transistor
MPP	Maximum Power Point
MPPT	Maximum Power Point Tracking
PID	Proportional-Integral-Derivative
PMA	Permanent Magnet Alternator
PMSG	Permanent Magnet Synchronous Generator
PPU	Power Processing Unit
PWM	Pulse Width Modulation
SIL	Software-in-the-Loop
VOC	Voltage Oriented Control
VSI	Voltage Source Inverter

List of Symbols

Symbol	Description	Unit if applicable
C_{min}	Minimum capacitance value	Farad [F]
D	Duty Cycle	-
f_e	Electrical frequency	Hertz [Hz]
f_{SW}	Switching frequency	Hertz [Hz]
I_O	Output current	Ampere [A]
I_I	Input voltage	Volts [V]
L_{min}	minimum inductance value	Henry [H]
n_s	Rotation speed	rotation per minute [rpm]
R	Resistance	Ohms [Ω]
S_1	Switch 1	-
V_O	Output voltage	Volts [V]
V_S	Source voltage	Volts [V]

Chapter 1

Introduction

The ever-growing demand for energy is a contemporaneous paradigm [1]. While seeking for energy sources, humanity has been using fossil energy sources, burning oil, altering landscapes to fit its needs. The Distributed Generation (DG) is a solution to minimize the impact of human thirst for energy, by producing energy on a smaller scale with renewable energy sources while closer to the end-user, thus minimizing environmental impact, as well as, electrical and economic losses.

The European Union, as a significant global influencer in environmental policies and regulations, has pushed forward the Directive 2009/28/EC [2], which promotes the use of energy from renewable sources [3]. This Directive has set targets for the year 2020 for all its member states, shown in Figure 1.1, some of them have already met theirs in 2017.

1.1 Distributed Generation

In [4], DG was defined as an electric power generation within distribution networks or on the customer side of the network. According to [2], it can serve business or homes, be part of a microgrid - electricity distribution systems containing loads and distributed energy resources, that can be operated in a controlled, coordinated way either while connected to the main power network or while it is islanded [5, 6].

When connected to low voltage utility, DG can support the delivery of clean, reliable power to additional customers and reduce electricity losses along transmission and distribution lines.

According to [7], the DG is getting wider attention, due to a larger uncertainty in demand and supply in the electricity regime. There are some key factors for it, taken from [7, 8]:

- Modularity and size;

- Shorter time frame needed for installation, when compared to conventional solution;
- Less chances of discontinuity of power supply;
- Flexibility to combine cost and reliability;
- Reduces system losses.

1.2 Renewable Energy

The renewable primary energy production produced in the European Union increased by two thirds during the period 2007-2017 [9]. Figure 1.1 shows the share of renewable energy sources from the EU Member States. Sweden's Energy mix has more than half of its shares made of renewable energy.

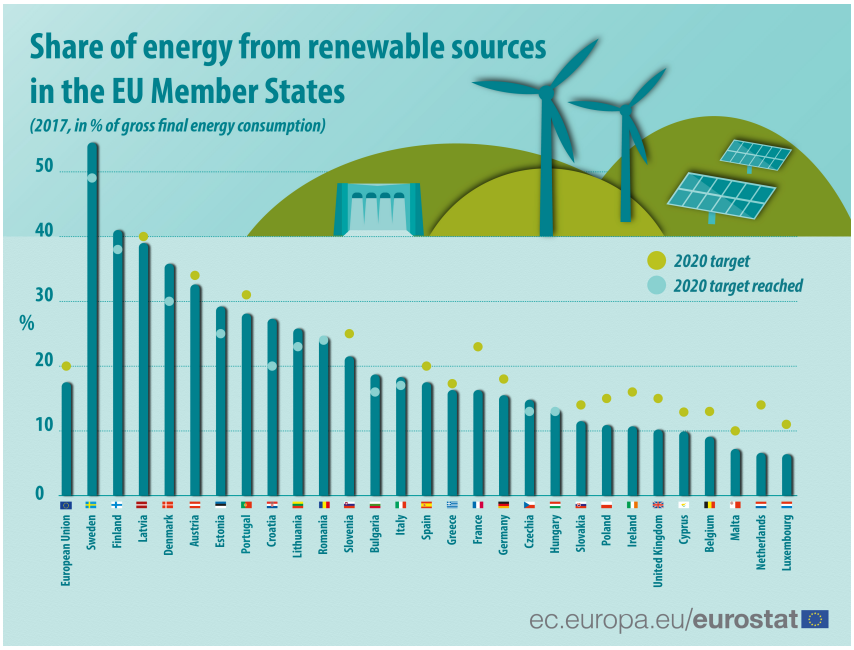

Figure 1.1: Share of energy from renewable sources [9].

Moreover, Figure 1.2 has the compiled data from 28 Member States of the European Union (EU-28) [9] and according to it, more than one quarter (30.7 %) of the electricity generation came from renewable sources. Furthermore, Wind power became the most important source, followed closely by Hydropower.

As shown in Figure 1.2, during the same time, solar power has been dramatically rising from just 3.8 TWh in 2007 to 119.5 TWh by 2017. Within ten years, the contribution of solar power to all electricity generated in the EU-28 from renewable energy sources rose from 0.7 % to 12.3 %.

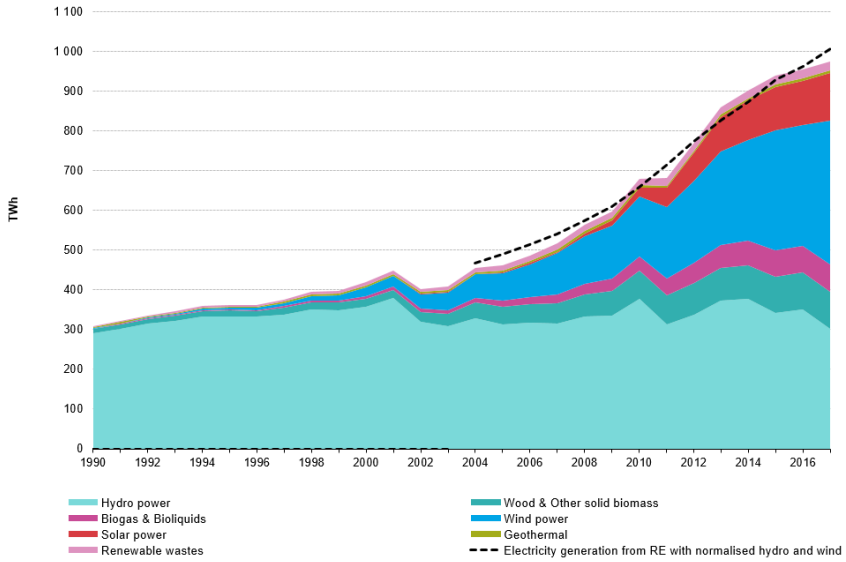

Figure 1.2: Gross electricity generation from renewable sources [9].

The technology related to the solar power has been receiving funding from governments across the globe to further reduce its costs [10]. Nowadays, the installation of low power (less than 1.5 kW) Photovoltaic systems and their connection to the grid can be done with off-the-shelf commercial inverters without the need of specially designed inverters [1]. The grid connection scheme of a solar system is represented in Figure 1.3.

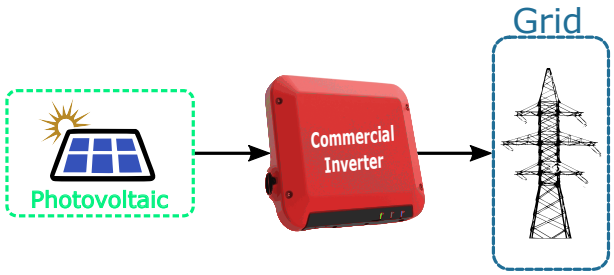

Figure 1.3: Illustration of the connection of a Photovoltaic source to the low voltage utility grid.

Pico-hydro is the smallest scale of Hydropower generation, and its capacity is less than 5 kW [11–14]. Pico-hydro can be owned by a single household [11, 13, 14], acting as the

energy supply in remote areas, mainly, in Developing countries [11–15]. According to [11, 13], among small scale renewable and conventional energy - e.g., small petrol and diesel generators - options for pico-hydro has been the most cost-effective so far, as it does not need neither fuel nor batteries, the payback period is shorter, it is affordable, and it has a flexible design [11–15].

In some Developing Countries, remote areas either do not have access to electricity due to the high cost of grid connection or, when they do, the power from the national electricity grid is unreliable [11, 13, 15]. Additionally, given the sufficient number of low head sites around the globe, these sites can offer significant sources for DG [11]. All these combined make developing countries a large pico-hydro potential market [11, 13, 14].

Although, the market for pico-hydro is not limited to developing countries, there is also a market for it in Europe, with the Directive 2009/28/EC and their renewable energy sources and sustainable generation [2, 16, 17].

Generators used in hydropower generation are generally connected to the grid, as depicted in Figure 1.4, but they rely on the control of the flow of water, or control of the turbine, to keep the generator in synchronization with the grid [11, 18]. The relation between the rotation of the turbine and the electrical frequency synchronization is going to be explained in the Chapter 2. For such a setup, it is better to have a constant flow of water all year round, otherwise its complexity increases.

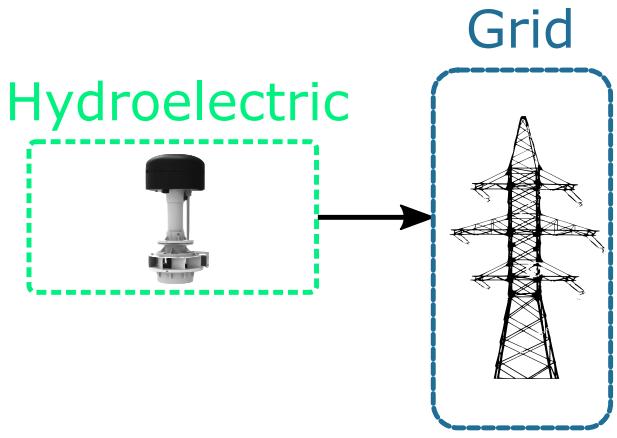

Figure 1.4: Illustration of a pico-hydro power source directly connect to the low voltage utility grid.

Different from what happens with Wind Power and solar power, there is no commercial

solution explicitly made for pico-hydro generation that can be bought off-the-shelf, typically, they are made on demand [19]. This thesis aims to propose a new power interface to bridge the already existing technologies of generator and Commercial Phtovoltaic Inverter (CPVI) and make them compatible.

1.3 Objectives

- Evaluation of a power interface between a generator, used in hydro and wind power generation, and an inverter in a Software-in-the-Loop (SIL) setup implemented in Matlab® Simulink®.
- Experimental validation and analysis with a Real-Time dSPACE Controller Board in a Hardware-in-the-Loop (HIL) test platform.

Chapter 2

State of the Art

2.1 Generator

The generator is coupled with a turbine, and converts the kinetic energy from the shaft into electrical energy [20–23]. There are different types of turbines, and they should be chosen based on specifications of the installation site [11, 20].

For electricity production, the Synchronous generator is typically employed in more considerable power plants, where the technical solutions required are more complex, and also more expensive, in such cases, the rotor is externally excited by a Direct Current (DC) source [20, 21]. Alternatively, it is also possible to use permanent-magnets rotors, eliminating the need for the DC supply. Such generators are termed as Permanent Magnet Synchronous Generators (PMSGs). The PMSG, then becomes a solution for electricity generation in remote areas, with no access to the utility grid, it has the advantage of being efficient, reliable, autonomous, and simple [20, 21, 24, 25].

The schematic diagram of a Three-phase AC machine is shown in Figure 2.1 to represent a cutaway view of a generator with a permanent-magnet excitation. While Fig. 2.2 shows the PMSG that is going to be used in the Experimental tests.

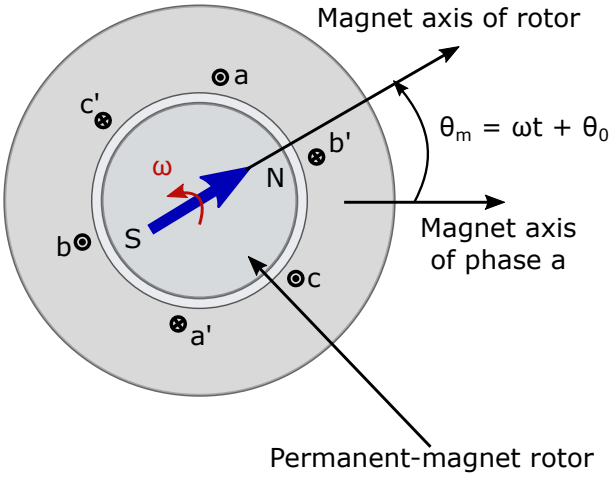

Figure 2.1: Schematic diagram of a three-phase permanent-magnet ac machine.

Table 2.1 presents the specifications of the two Permanent Magnet Alternators (PMAs), also known as PMSG. firstly, the 60-2s-7p, shown in Fig. 2.2, was used during the Software-in-the-Loop (SIL) and the Hardware-in-the-Loop (HIL). The former was used as a reference for simulated generator, the latter was used directly as the generator for all experimental tests. The second, 100-14s-1p, was used for the design of the Cúk Converter. Both of these, sold by [26] for “do it yourself (DIY) projects", are used as PMSGs for this thesis.

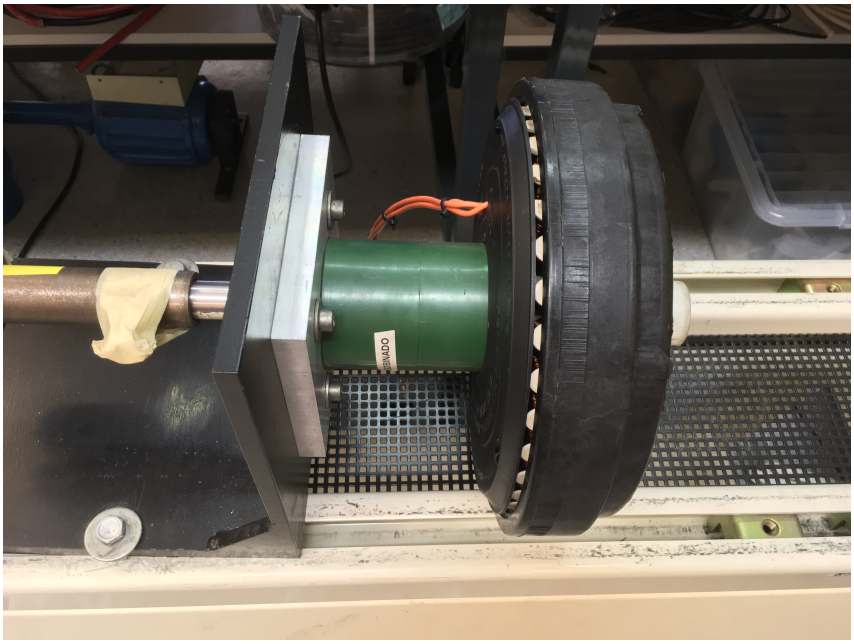

Figure 2.2: Photo of 60-2s-7p generator.

Table 2.1: Technical data for the Generator at 1600 rpm.

Generator model	Connection	V/rpm	W/rpm	$V_{DC_{OC}}$ [V]	V_{DC} [V]	P [W]	I [A]
60-2s-7p	Star	0.15	up to 1	240	163.4	<1600	<11.1
100-14s-1p	Star	0.27	up to 1	432	259.2	<1600	<6.2

Figure 2.3 shows the Torque vs. Speed and Power vs. Speed curves of hydro turbine. For each speed there is a pair of Torque and Power associated with it, i.e., for each flow of water flowing through the turbine there is angular velocity of the turbine, and, as a consequence, its respective electric power amount [20, 25, 27].

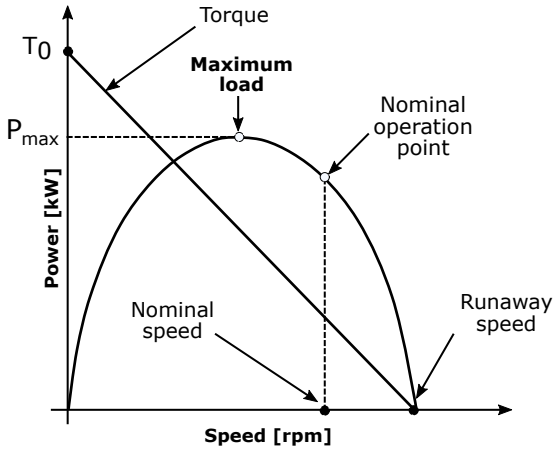

Figure 2.3: Torque and Power as a function of speed for a hydro turbine [27].

For the generated electricity at the output terminals of the PMA, has a corresponding frequency (f_e), which depends on the rotation speed of the turbine (n_s). Equation (2.1) shows the algebraic relation between the electrical frequency (f_e), in Hertz, rotation speed (n_s), in rpm, and the number of poles (p) [21, 23].

$$f_e = \frac{n_s \cdot p}{120} \tag{2.1}$$

After being built, the number of poles is fixed, so the frequency of the voltage output is proportional to the rotational speed of the turbine, so to connect such generator to the utility

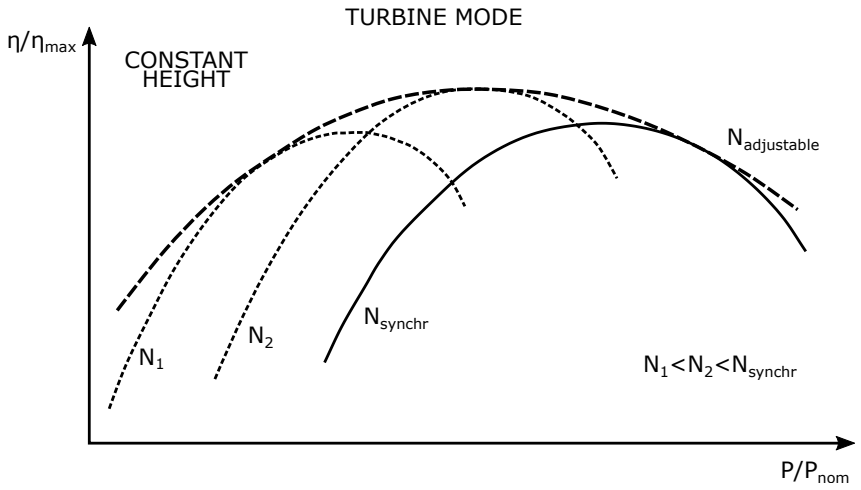

Figure 2.4: Variable Speed [27].

grid, it is necessary to make sure that frequency and voltage comply with the standard set by the Standard Organizations, e.g., 50 Hz in Europe or 60 Hz in Brazil [28, 29].

With that in mind, turbines made for power plants are designed to be optimized for a specific set of rotation speed, head, and water flow, in short, they must operate at fixed speed to respect electrical energy standards to prevent grid desynchronization [18, 28, 29].

When operating at fixed speeds any change in water flow will force the generator to operate with a lower efficiency at a non-optimal power point [18, 27]. Power electronics enables the turbine to operate at Maximum Power Point (MPP) for varying speeds. Figure 2.4 depicts this idea [27].

Figure 2.5 shows a generic voltage-current curves for a rectified PMSG [1, 19]; For each speed there is a curve with its respective MPP.

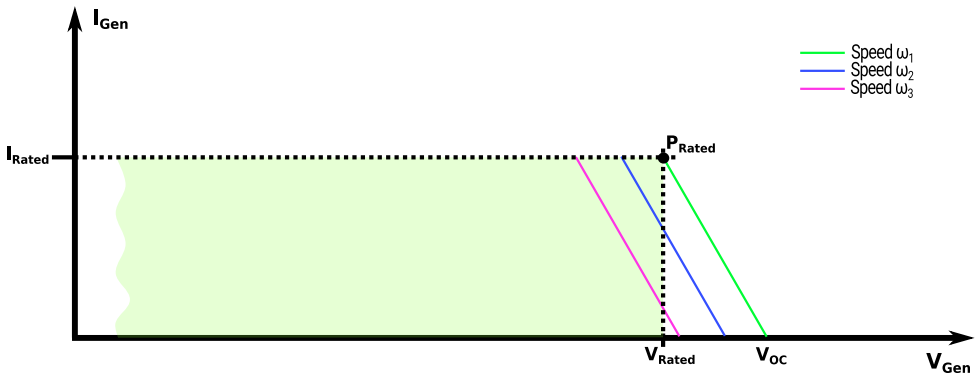

Figure 2.5: Rectified Generator Current-Voltage Curves.

2.2 Commercial Photovoltaic Inverters

Figure 2.6 shows two Commercial Phtovoltaic Inverter (CPVI) from two different manufacturers. While Figure 2.7 shows a diagram of a generic power structure used to connect Photovoltaic strings to the Utility Grid. Low power PV modules have low output voltages, so they need a boost converter stage before the inverter [30, 31]. All CPVIs must comply with power quality standards [28, 29].

Figure 2.6: PV inverters: Omniksol-2k-TL2 (on the left) and SB 1.5-1VL-40 (on the right).

In [31], the power structure topology of different CPVI manufacturers is described. It also provides some insight into a generic control strategy, as well as some basic functionalities. These ideas are depicted in Figure 2.8.

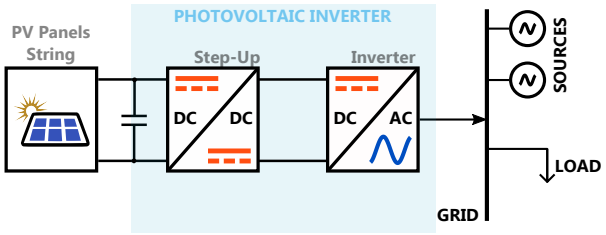

Figure 2.7: Schematic of PV String connected to the Grid.

As depicted in Fig. 2.8 [31], the basic functionalities of a CPVI includes: Maximum Power Point Tracking (MPPT), to extract the maximum power available from the PV String, the boost

is responsible for controlling input (the V_{PV} voltage or I_{PV} current), while at the same time, the inverter is extracting power from V_{DC}, as much as possible, to supply energy to the utility grid, by controlling its output current, I_g. They are also capable of controlling/managing a Microgrid, as well as support the network by compensating power factor, frequency, voltage, and reactive power. A low pass filter is also present to reduce harmonics and higher frequency noise.

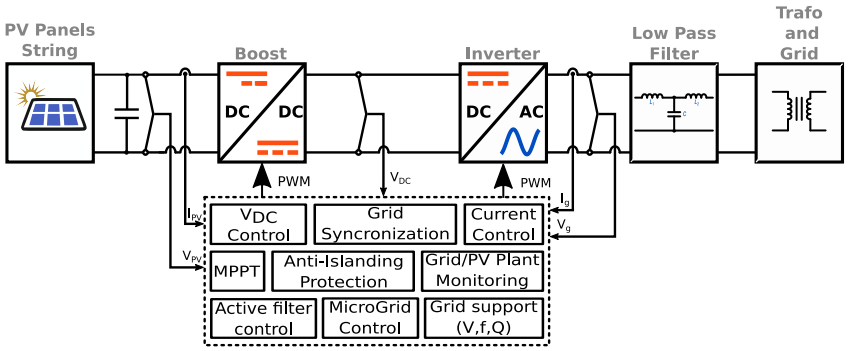

Figure 2.8: Generic structure of a Commercial Photovoltaic Inverter with a boost converter stage.

2.2.1 Characteristics of Commercial PV Inverters

Some generic commercial PV Inverters topology elucidated previously on Figure 2.8 are listed in the Table 2.2, with their characteristics taken from their respective manuals [30, 32–34], maximum DC power and voltage, operating range of the MPPT algorithms and other characteristics. Such information will be relevant to analyze the results of the experiments.

Table 2.2: Commercial Photovoltaic inverters.

Type	Omniksol-2k-TL2	Piko MP Plus 1.5-1	SB 2100TL	Solax X1-1.5-S-D
Maximum DC Power [W]	2,300	1,540	2,200	1,650
Maximum Input Voltage [V]	500	400	600	400
Rated DC Voltage [V]	360	350	400	360
MPPT Voltage Range [V]	120-450	75-360	125-480	70-380
Minimum Input Voltage [V]	120	75	125	70
Start up DC Voltage [V]	150	75	150	70
Maximum DC Current [A]	18	13	12	10

The efficiency curve of the SB 2100TL, from SMA [33], is shown in Fig. 2.9, and it is important to notice that the maximum efficiency occurs for the Rated DC Voltage, 400 V, available at Table 2.2.

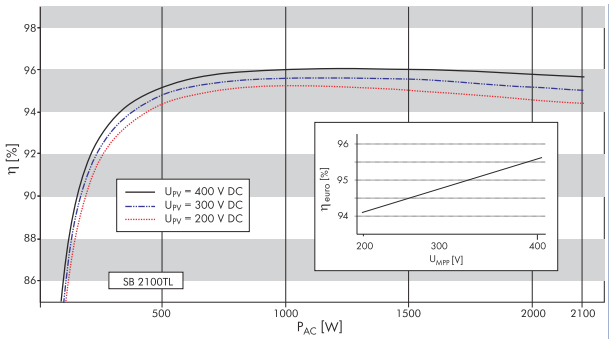

Figure 2.9: Efficiency curve of SB 2100TL.

2.2.2 Maximum Power Point Tracking Algorithm

Figure 2.10 shows generic Current-Voltage (IV) Curves of PV String along with the limiting characteristics of a CPVI. The MPPT algorithm sweeps through Current Voltage pairs, scouring for the MPP within those limits. The algorithm chosen for this thesis is the Perturb & Observe (P&O), which is the most common, and it is widely used in PV application [35–38].

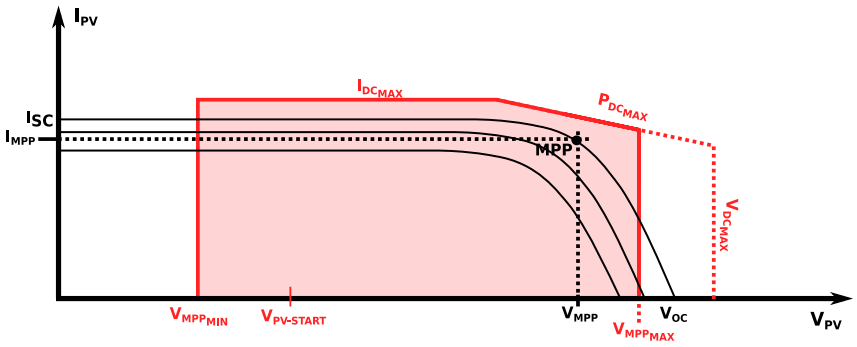

Figure 2.10: Photovoltaic Inverter IV Curve.

The P&O algorithm usually works by sensing either the Open-Circuit Voltage and/or the Short-Circuit Current, to estimate a start point, then it continuously sense the Voltage and Current[35], then calculates the power, followed by the analysis of the current power and previous power, then it decides if it should either increase or decrease the reference. The flowchart of the P&O algorithm is shown in Fig. 2.11 [35–38].

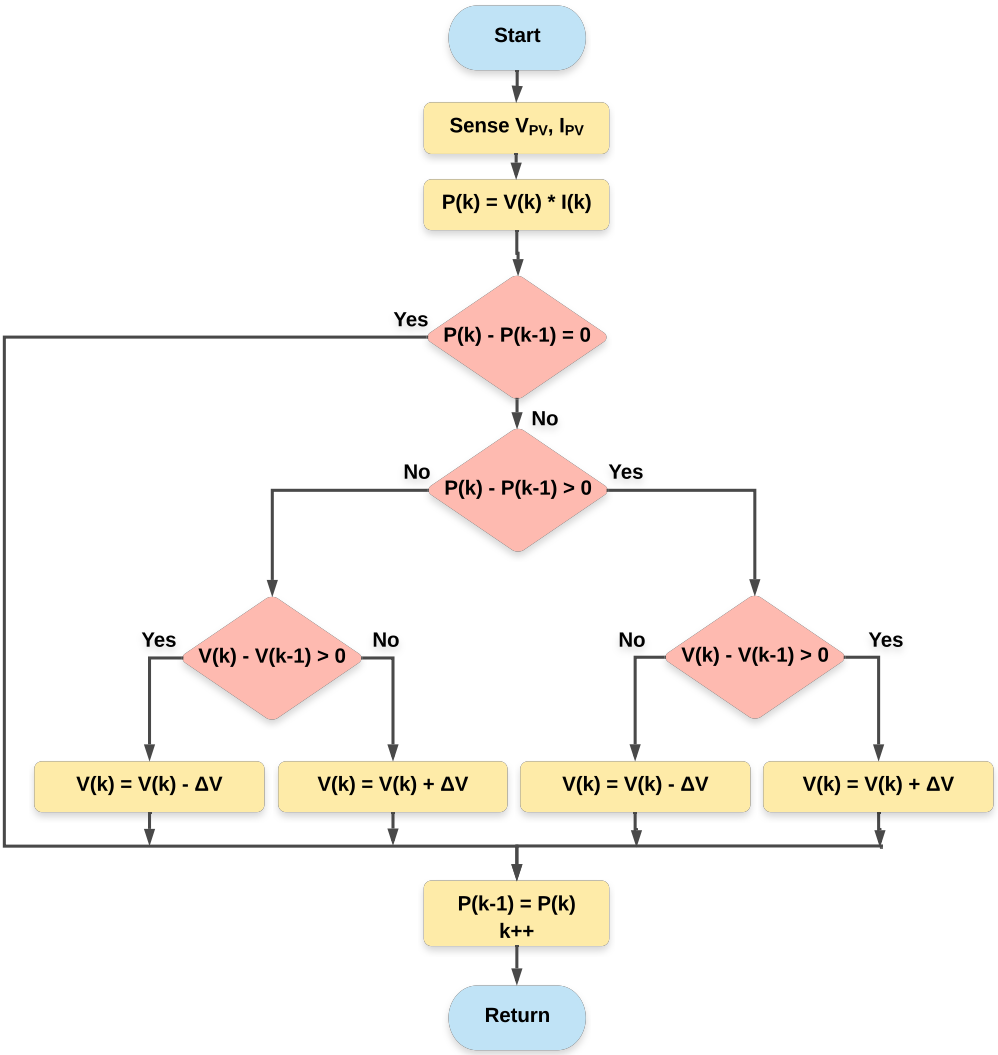

Figure 2.11: Peek and Observe Algorithm for MPPT.

2.3 Current Status

As proposed by [1, 39], the possibility of connecting a PMA to a commercial PV inverter has been exhaustively tested, and with a pair of well-matched rectified PMA and PV inverter, it is a viable alternative. Figure 2.12 shows the result of the reproduction of their experiment.

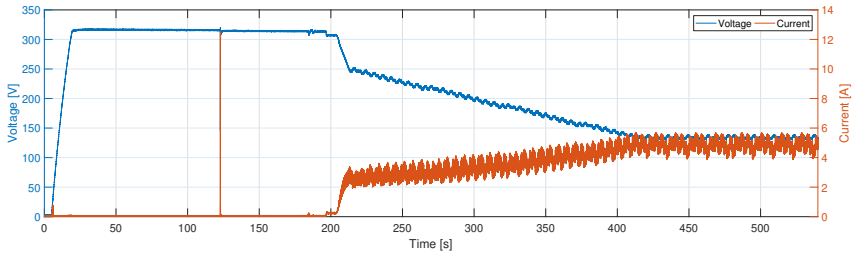

Figure 2.12: Rectified voltage and current of the PMA connected to SB 2100TL CPVI.

At the instant 125 s of the Fig. 2.12, there is a peak current, which suggests that the MPPT algorithm sensed the short-circuit current, then the pv inverter started working. After some time, it reached the steady state, at the lower voltage limit of the MPPT range operation [33].

Ribeiro, Maidana, Leite, and Ferreira, in [40], tested the connection of a low power generator (300 W) with microinverters, which also had a positive response. Their results proved the feasibility of using a microinverter for a pico-hydro, but the maximum power extracted was for the passive load test, instead of the microinverters used, which demonstrated that the MPPT algorithm employed by the microinverters manufacturers is not a perfect match for such application, consisting of a water wheel prototype, generator and microinverters.

The Power Spout Company has also been testing the feasibility of using PV inverters to connect the PMA to the grid, and they have documented which models are compatible with their catalog [41]. They have also developed a commercial overprotection module, Fig. 2.13, to account for the differences between the solar power generation and hydropower generation, such as no-load situations or excess water flow conditions.

In [42], they have prototyped a low-cost overvoltage protection module, made using analog components such as the PMW generator TL494 [43], promoting the use of this technology concept.

Figure 2.13: Overvoltage Protection Module for Hydropower generation sold by [26].

The setup depicted in Fig. 2.14 shows the schematic of what have been tested so far by [1, 39, 40, 42]. The differences between these previous applications lies in the power scale, but the applied concept is still the same, using commercial components to provide an effective solution to connect PMSGs to the utility grid.

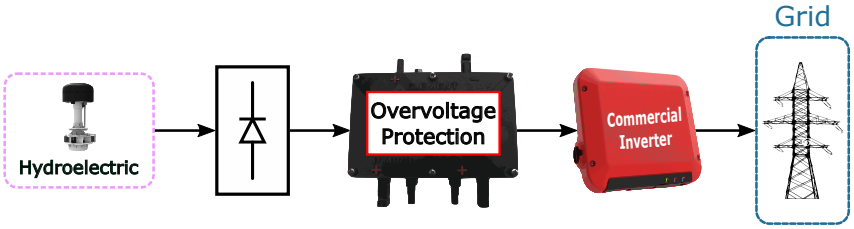

Figure 2.14: Configuration that has already been test.

Chapter 3

Methodology

This chapter introduces the Power Processing Units proposed to solve the existing compatibility problem between Permanent Magnet Synchronous Generator (PMSG) and commercial Photovoltaic Inverter. The modeling of the Power Processing Units (PPUs) studied are based on discrete-time domain analysis using Matlab® Simulink®. The fundamentals of this approach are further elaborated in this section. Simulation and experimental results are used to verify the proposed approaches.

3.1 Proposed strategy

The experiment made by [1] when emulating a Commercial Phtovoltaic Inverter (CPVI) yielded promising results. They did not implement a voltage-controlled boost converter, as done by [44], instead they adopted a current control strategy. This approach, when applied to a rectified pico hydro PMSG, enables the generator plus the Current-Controlled Boost Converter (CCBC) paint to work as a Current Source, i.e., this composition emulates the operation of a Photovoltaic array. Thus creating an ideal scenario for employing CPVIs. The Figure 3.1 depicts a block diagram of systems with the proposed topology.

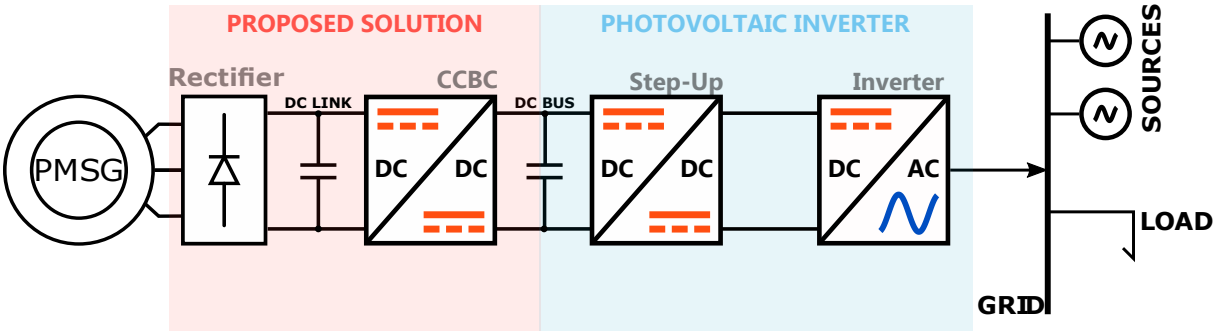

Figure 3.1: Proposed solution block diagram.

This current control strategy allows the DC/DC converter to be used in pico hydro generation systems [1], where the CCBC acts as a power interface between the generator and the inverter. This idea is illustrated in the diagram shown in Figure 3.2.

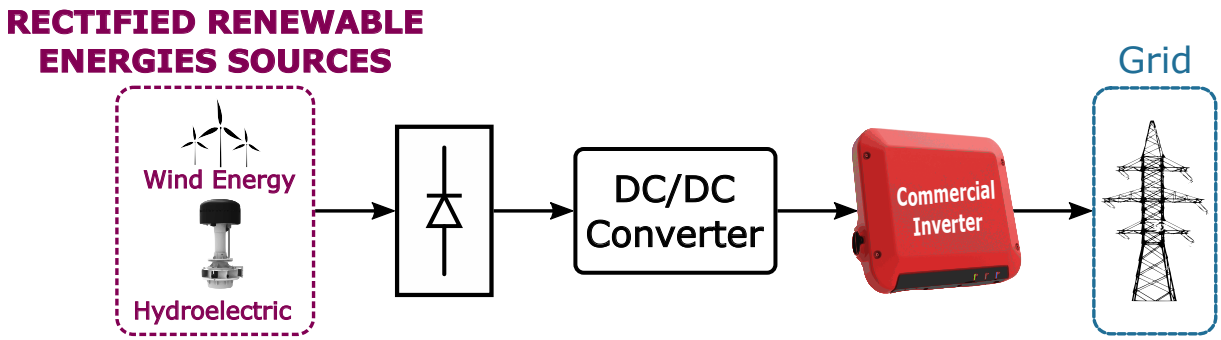

Figure 3.2: Wind and Pico hydro energy sources being connected to the utility grid.

3.2 Power Interface

This section provides an overview of the power structures as well as the controlling of each topology implemented.

3.2.1 Boost Converter

The Figure 3.3 shows a step-up converter, when the switch S_1 is off. This converter is also known as boost converter. As the name implies, the output voltage IV_O is always higher than its input voltage V_S. Its main application is in regenerative braking of DC motors, and regulated dc power supplies [45, 46], because of the latter application this converter was chosen.

When the switch S_1 is on. the Diode D_1 is reversed biased, thus isolating the Capacitor C_O, which supplies the Load. During this time, the inductor L_1 is being charged by the Source S and the current returns through the switch S_1, as illustrated in Figure 3.3 [47].

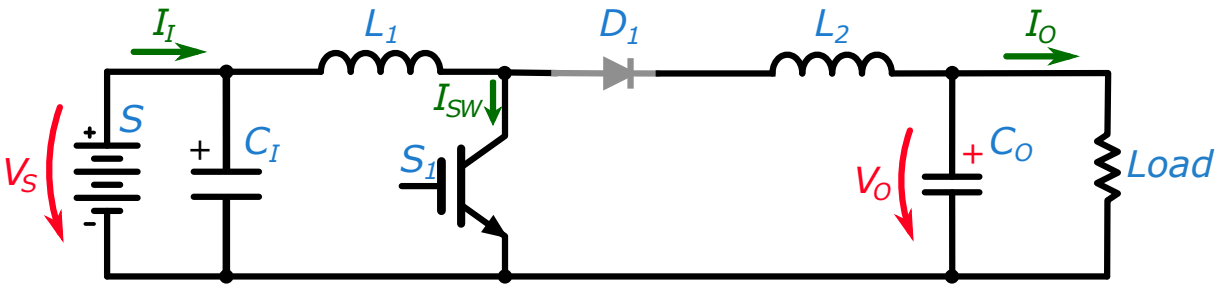

Figure 3.3: Boost Converter Diagram.

Figure 3.4 shows the time when the switch S_1 is off. When this happens, the inductor L_1 plus the source, S, supply energy to the Capacitor C_O and the Load, while the capacitor C_O ensures a constant voltage with low ripple ratio.

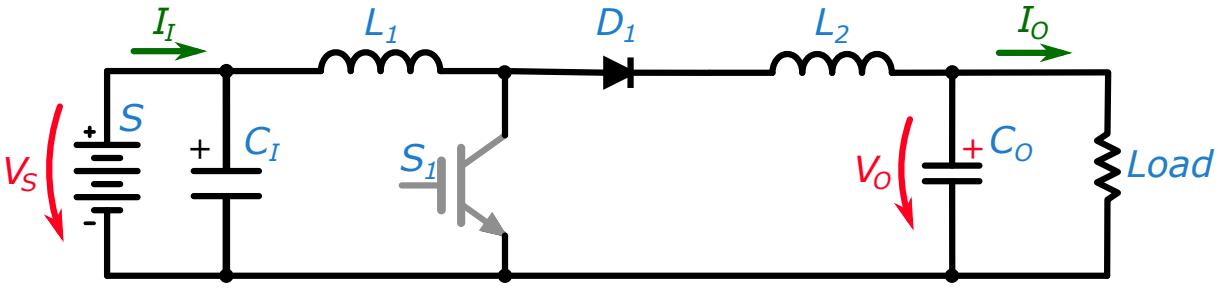

Figure 3.4: Boost Converter Diagram when switch S_1 is off.

The inductor L_2 filters the I_O current supplying the load with a DC current with low ripple ratio, but for this project the load is a commercial PV Inverter, provided that said inverters are voltage controlled in its input, as seen in Figure 2.8, it is not mandatory to include the inductor L_2 in the experiment as the capacitor C_O is enough to provide a stable voltage to the PV inverter.

As the boost converter is a DC/DC switching converter, its gain curves follow the generic gain curve shown in Fig. 3.5. In an ideal scenario, there would be no losses, so, it would be possible to obtain an infinite gain, but contrarily, due to parasitic losses, gain reaches a maximum, then it starts losing its efficiency. The dashed lines, both blue and red, represents the poor switch utilization at high values - close to 1 - of Duty Cycle [45].

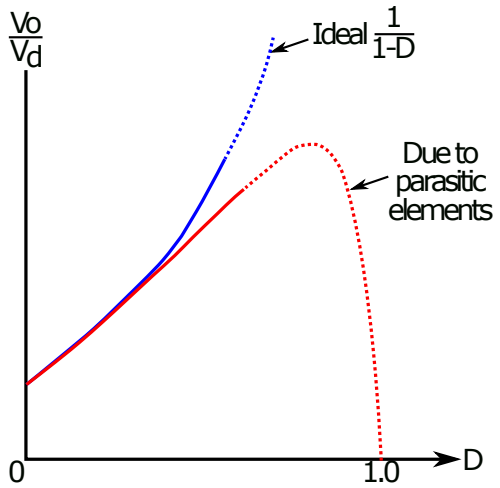

Figure 3.5: Generic gain curve of a Boost Converter [45].

The equations for the design of the Boost converter, with no capacitor at the input nor an inductor at the output, are described in Equations (3.1)-(3.3), where, V_O is the output voltage, V_S is the source voltage, D is the duty cycle, R is the Load resistance, f_{SW} is the switching frequency, L_{min} is the minimum inductance value, C_{min} is the minimum capacitance value, and $\Delta V_O/V_O$ is the acceptable ripple ratio [19, 45–47].

$$V_O = \frac{V_S}{1-D}, \tag{3.1}$$

$$L_{min} = \frac{D \cdot (1-D)^2 \cdot R}{2 \cdot f_{SW}}, \tag{3.2}$$

$$C_{min} > \frac{D}{R \cdot f_{SW} \cdot \frac{\Delta V_O}{V_O}}. \tag{3.3}$$

$$\tag{3.4}$$

The designed components were used for the Simulation test, shown in Table 3.1, while, due to time constraints and resources available at the laboratory, for the Hardware-in-the-Loop (HIL) the magnitudes used are shown in Table 3.2.

Table 3.1: Data for the simulation of the Boost converter in the Software-in-the-Loop (SIL) test.

Variable	Magnitude
Switching frequency	10~kHz
Capacitance	1~mF
Inducante	12~mH

Table 3.2: Data for the HIL test.

Variable	Magnitude
Switching frequency	10~kHz
Capacitance	1~mF
Inductance	12~mH

3.2.2 Ćuk Converter

The DC-DC converter shown in Figure 3.6 was named after its inventor, Ćuk [48]. The Ćuk converter provides an output voltage magnitude that is either greater or smaller than the input voltage magnitude, said output is negatively polarized with respect to the common terminal [45, 46]. The Ćuk Converter, was chosen because of its characteristics of being able to boost or decrease the current, depending on the Duty Cycle, D, and also for the fact that the current is continuous in both the input and the output.

Equations (3.5) and (3.6) describe, mathematically, the relation between the input and output current and voltage [45–47, 49].

$$\mathrm{I}_O = \frac{\mathrm{I}_I \cdot (1 - \mathrm{D})}{\mathrm{D}}, \tag{3.5}$$

$$\mathrm{V}_O = \frac{\mathrm{V}_S \cdot \mathrm{D}}{1 - \mathrm{D}} \tag{3.6}$$

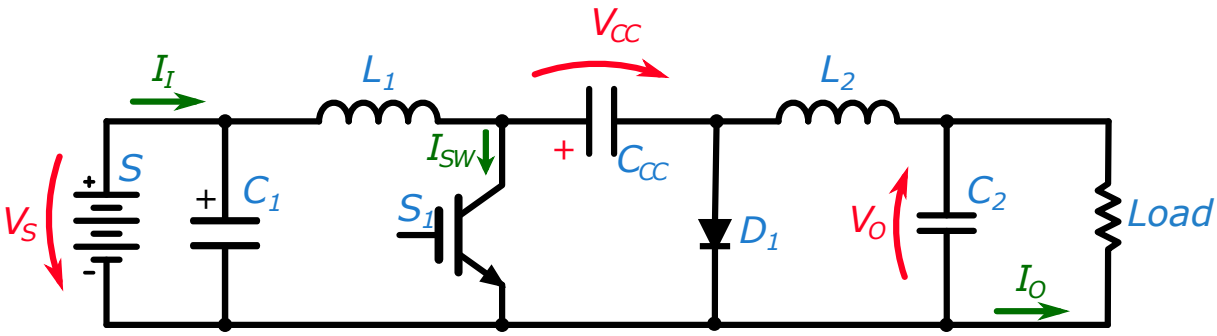

Figure 3.6: Ćuk Converter when switch S_1 is on.

The Capacitor C_1 is the primary means of storing and transferring energy from the input to the output [45]. Equations (3.7) and (3.8) are used to design the input Capacitor and its Equivalent Series Resistance (ESR), respectively [49].

$$C_1 = \frac{I_O \cdot r_2 . \cdot D}{8 \cdot (1 - D) \cdot f_{SW} \cdot V_{O_{ripple}}} \tag{3.7}$$

$$ESR_{Input} = \frac{V_{O_{ripple}}}{I_O \cdot r_2} \tag{3.8}$$

When the switch S_1 is turned off, illustrated in Figure 3.7, the currents from inductors L_1 and L_2 and flows through the Diode D_1. While this happens, the Coupling Capacitor C_{CC} is being charged by the energy stored in L_1 and C_1. At the same time, the output is being fed by L_2 and C_2.

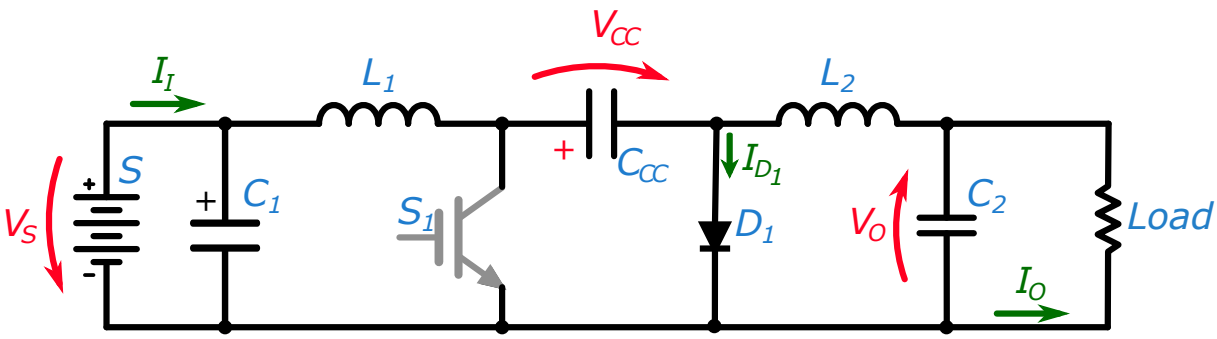

Figure 3.7: Ćuk Converter when switch S_1 is off.

Equations (3.9) and (3.10) are used to design the inductors L_1 and L_2, respectively [49].

$$L_1 = \frac{V_S \cdot (1 - D)}{I_O \cdot r_1 \cdot f_{switching}}, \tag{3.9}$$

$$L_2 = \frac{V_S \cdot D}{I_O \cdot r_2 \cdot f_{switching}}. \tag{3.10}$$

As this converter is made of basically a boost converter at the input plus a buck converter at the output, and both of these are connected by the C_{CC}, which acts as an intermediary energy storage. The design is made based on Equations (3.11) [49].

$$C_{CC} = \frac{I_O \cdot (1 - D)}{D \cdot f_{switching} \cdot V_{Cs_{ripple}}}, \tag{3.11}$$

The output capacitor C_2 and its ESR are calculated by Equations (3.12) and (3.13) [49].

$$C_2 = \frac{I_O \cdot r_2}{8 \cdot f_{switching} \cdot V_{O_{ripple}}}, \tag{3.12}$$

$$ESR_{Output} = \frac{V_{O_{ripple}}}{I_O \cdot r_2}. \tag{3.13}$$

Table 3.3 presents the designed values used for the simulation of the Current-Controlled Ćuk Converter (CCCC) tests. Note that the Ćuk converter was designed to operate at a switching frequency of 20 kHz, as it will not be implemented in the HIL test platform.

Table 3.3: Specifications of the CCCC converter implemented.

Variable	**Magnitude**
Switching frequency	20 kHz
Nominal input current	8 A
Input Capacitor	6.39 µF
Coupling Capacitor	20.9 µF
Output Capacitor	281.9 nF
Input Inductor	8.9 mH
Output Inductor	12.9 mH

3.2.3 Control algorithms

The power structure for the SIL experiment is divided into two independent structures, the Step-Up Converter and the Commercial Voltage Source Inverter (CVSI) emulation. The Step-Up converter is Current Controlled, henceforth, CCBC similarly to [19], and the CVSI uses a voltage control algorithm for the DC/DC stage and Voltage Oriented Control (VOC) control strategy, extracted from [44], for the DC/AC stage. An overview of the power structures for the boost converter and the Ćuk converter, as well as the controllers, are shown in Figures 3.8 and 3.9. VOC extracts the voltage phasor of the grid, i.e., it obtains the aplitude of the Grid Voltage and

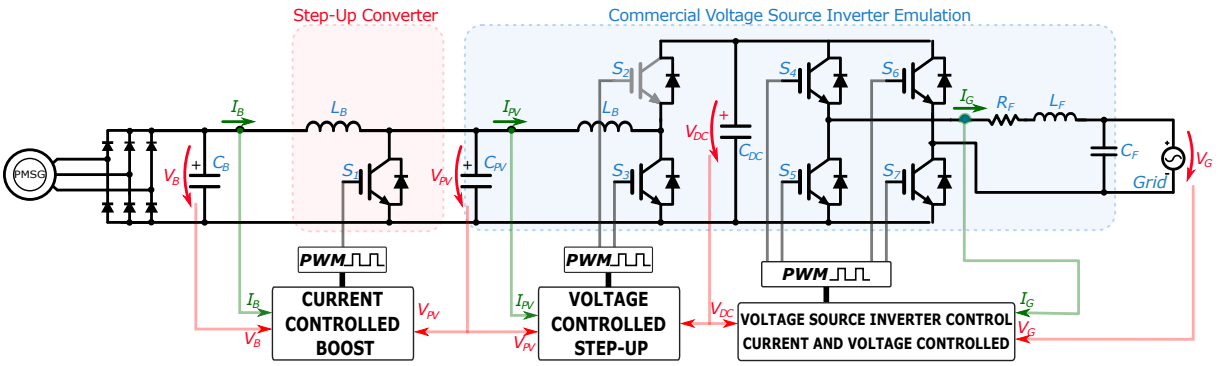

Figure 3.8: Power and control overview for the boost converter.

its phase, hence the name. Later, these values are supplied as references for the controllers. By controlling the phase of the current being supplied by the inverter, it is possible to choose between adjusting the power factor of the grid, either lagging or leading, or merely supplying active power.

This controller works in the direct-quadrature domain. In which the AC waveform is being projected onto a rotating two-axis reference frame, synchronous and with the direct axis aligned with the grid voltage phasor. In this case, voltage and current components become DC signals related to the two rotating axis. This simplifies calculations and allows the use of Proportional-Integral-Derivative (PID) controllers, as the latter do not work well for sinusoidal variables.

This simulation setup was previously validated through HIL experiments by [1, 19], when it used a current-controlled step-up converter plus an inverter, both implemented in a Real-Time Controller Board system, to connect a pico hydro generator to the electrical grid.

The Step-Up controller receives the measurements for V_B and I_B, as these are used for the Maximum Power Point Tracking (MPPT), but it is mainly responsible for keeping the current I_B at the reference value. Furthermore, as a protective measure, it is also responsible for ensuring that the voltage V_{PV} stays within an acceptable range to prevent damaging the inverter.

The VOC is responsible for keeping the V_{DC} constant, by extracting the energy stored in C_{DC} and supplying it to the utility grid, by controlling the grid current, I_G, as grid voltage, V_G, is set by the utility grid.

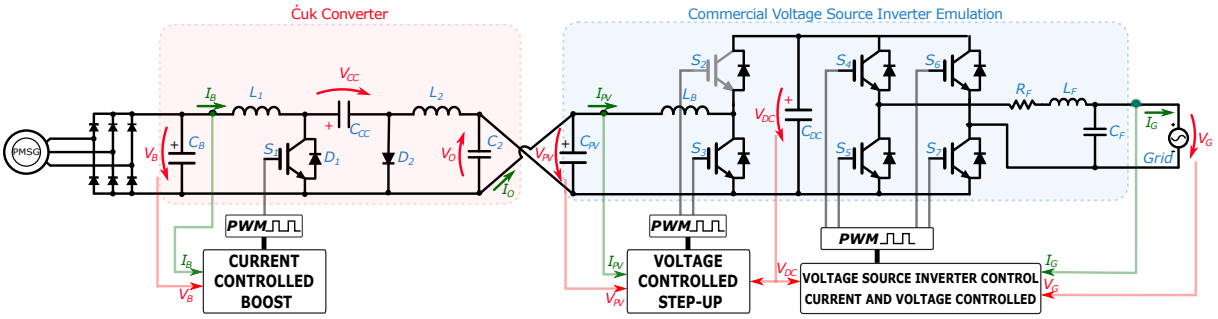

Figure 3.9: Power and control overview for the Ćuk converter.

Similarly, the power structure of the HIL experiment is shown in Figure 3.10, but instead of using an inverter emulation, as in Figure 3.8, the experiment consisted of connecting the CCBC to a commercial PV inverter. Both SIL and HIL emperiments were designed to work in a discrete-time domain, with a simulation step of 20 µs, while almost all controllers work on a 0.1ms step, with the exception being the controller for the CCCC, which runs in steps of 50 µs.

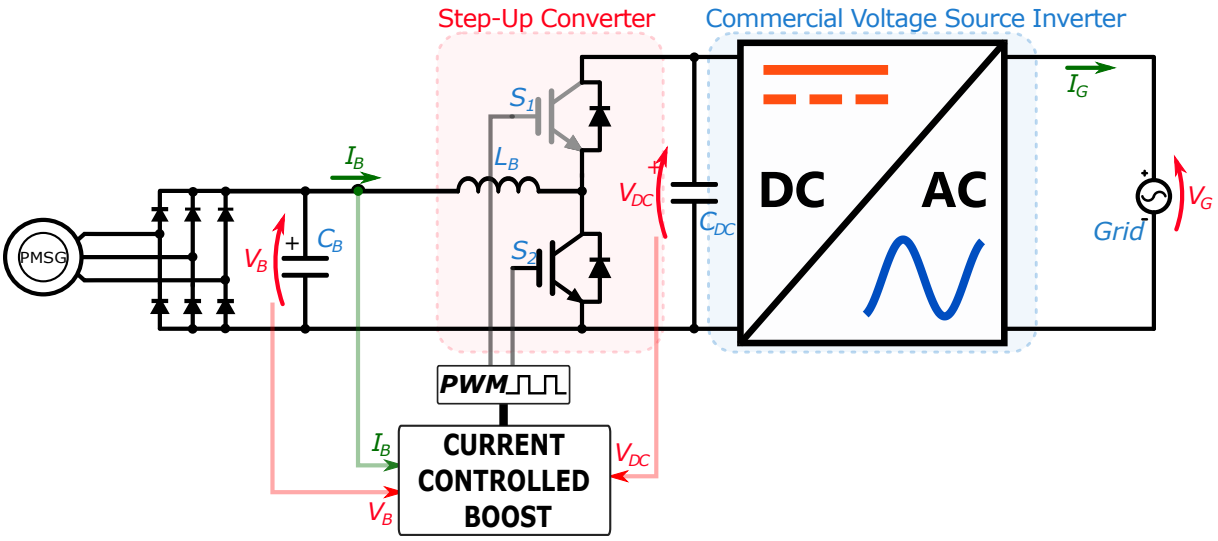

Figure 3.10: Power and control overview for the HIL.

The proposed control strategy for the CCBC in the HIL platform is represented in Figure 3.11. It receives the input voltage and current, and output voltage, V_B, I_B and V_{DC} respectively. It is possible to select if the current set-point, I_B^*, is going to be supplied by the MPPT algorithm or if it is going to be manually set. While the control strategy implemented for the SIL experiments, for both CCBC and CCCC, is represented in Figure 3.12, where I_B^*, is manually set.

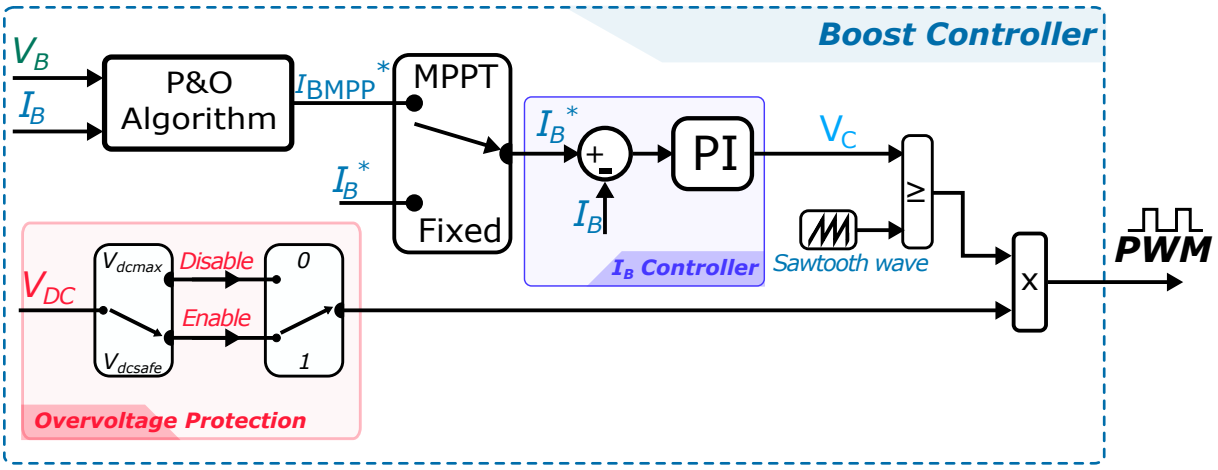

Figure 3.11: Controller overview for the HIL test.

Afterwards, I_B is compared to the set-point, then the PI Discrete-time Controller will work to minimize the error and outputs the control signal V_C which is compared to a Sawtooth wave of

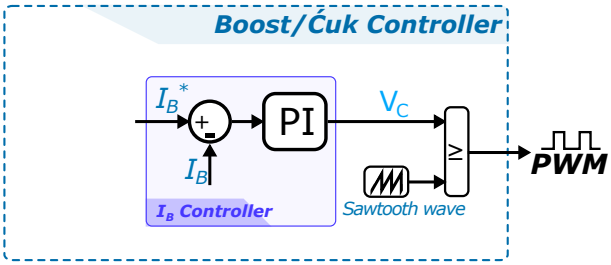

Figure 3.12: Controller overview for the SIL test.

10kHz, generating the Pulse Width Modulation (PWM) signal to switch on/off the Insulated-gate Bipolar Transistors (IGBTs).

The Over-voltage Protection checks if V_{DC} respects the maximum input voltage for the PV Inverters shown in Table 2.2 and, if yes, then it keeps Step-Up enabled, otherwise, it disables the PWM until the voltage reaches a safe value, V_{dcsafe}.

Proportional-Integral-Derivative Control

Proportional-Integral-Derivative Control (PID) refers to a control method widely employed in several applications, due to its relatively low complexity, robustness and ease of use. It is named after its three components: the proportional, integral, and derivative. Each of these terms tries to minimize the error, i.e., the difference between the measured value and the desired value for a process variable. The desired value is called set-point of the controller, while the output of the controller is called the control variable [50, 51].

The implemented control structure can be seen in Figure 3.13. The proportional component determines how fast the response of the controller will be once a difference between the set-point and control variable has been detected. Setting higher values of gain causes a faster dynamic response; however, the system may become unstable. The proportional component alone cannot entirely eliminate the Steady-State Error. Solving that problem requires an integral component, which produces an output proportional to the error integrated over time. This component eliminates the steady-state error, but it will also correspond to a more substantial settling time [50–52].

One of the integral component's significant drawbacks is evident in practical applications,

where, e.g., the output of the controller is limited and unable to control the desired variable properly. In those cases, saturation of the integral component might occur, and thus, even though the error might be small, due to the accumulated error the controller's output deviates from the set-point. This issue can be overcome with a anti-windup integrator, that is, one with a limit for the integration and a integral reset function [52]. The derivative component does not act on

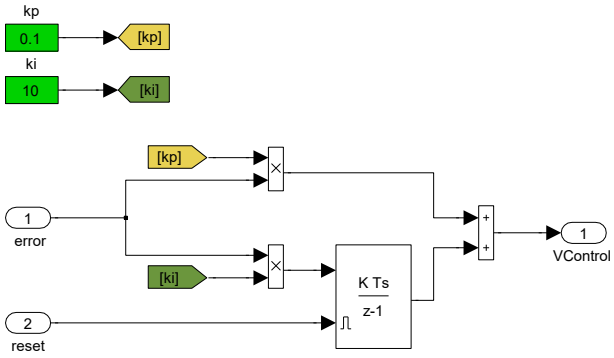

Figure 3.13: PI controller used in the SIL and HIL.

the value of the error itself, rather on its rate of change. The derivative component will produce an output proportional to that change. One of its drawbacks is the sensitivity to high-frequency signals. As in the literature,in this work, only the Proportional and Integral (PI) components were implemented, as can be seen in Fig. 3.13, where kp is the proportional gain and ki is the integral gain.

3.3 Simulation-in-the-Loop

The SIL experiment was done trying to mimic the HIL as close as possible, to enable the detection of possible issues and work on them. For the SIL tests were made for the Boost Converter as well as for the Ćuk converter. The Control algorithm is similar for both of the DC topologies.

All the parameters used in the simulation were the same as the ones of the components available at the laboratory, from the specifics of the generator, Table 3.4, to inductors, switches, and capacitors available. The SIL experiment does not contemplate the overvoltage protection and MPPT features from the diagram, and the implemented controller is shown in Fig. 3.12.

The parameters used for the CCBC and CCCC are shown in Tables 3.1 and 3.3, respectively.

3.4 Hardware-in-the-Loop

For this experiment, the 60-2S-7P Permanent Magnet Alternator (PMA), shown in Figure 2.2, from [26]. Its stator is composed of the parallel of seven (7P) series of two windings (2S), which are made of a cable with a diameter of 0.6mm (60), hence the name 60-2S-7P. In the end this 2 HP, i.e., 1491.39 W, generator has 42 windings in total. Its characteristics are shown in Table 3.4.

Table 3.4: Technical Data of the generator 60-2S-7P at 1600 rpm.

V/rpm (OC)	**W/rpm (DC)**	**VLL [V]**	**$V_{DC_{OC}}$ [V]**	**V_{DC} [V]**	**I_{DC} [A]**	**P [W]**	**$I_{Generator}$ Wye [A]**	**Pair of Poles**	**R between phases**
0.15	0.9	122.2	233.3	163.4	8.6	1410.1	6.45	28	0.9

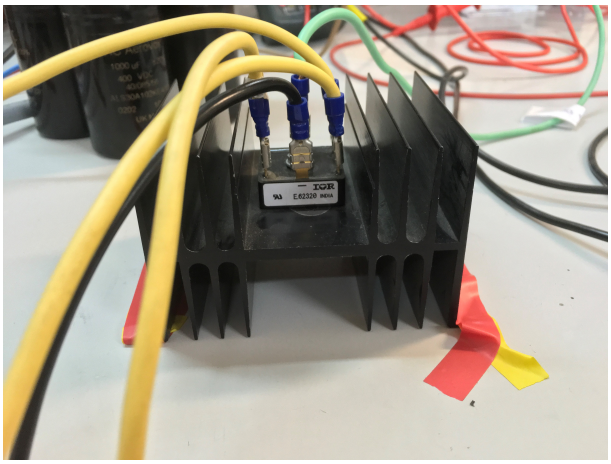

Figure 3.14: Bridge Rectifier attached to a heatsink.

Figure 3.15 shows the implemented setup. It consists of an ABB ACS355 frequency converter driving a three-phase motor to supply mechanical power to the 60-2S-7P generator. The latter is then connected to the bridge rectifier E62320, shown in Figure 3.14, which is then connected to the DC Coupling, a capacitor bank of 1 mF capacitance. Later, the DC Coupling connects to the CCBC, and the latter is connected to a DC Bus, which is also a capacitor bank of 1 mF. Then, a Commercial PV Inverter extracts power from the DC bus and injects it into the laboratory's grid.

It is important to note that the ABB ACS355 [53] was configured to limit the maximum speed to 1600 rpm, as a precaution, so that there would not occur an overvoltage, which would damage the equipment.

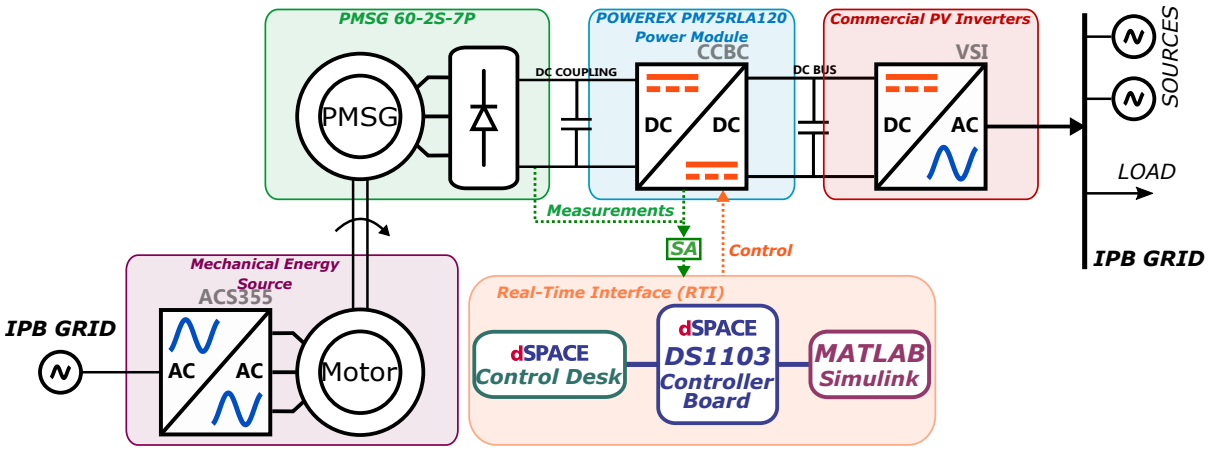

Figure 3.15: Experimental setup overview.

Voltage and Current probes are set to measure the input and output voltages and currents for the CCBC. These measures are then filtered and digitized in the Signal Acquisition Module (SA), and are then transmitted to the dSPACE DS103 Controller Board which is connected to the computer. In the computer the dSPACE ControlDesk loads the designed model built-in Matlab® Simulink® and the data from the controller board. This software, Figure 3.16, allows the user to interact with the power structure in real-time, the parameters that are meant to be interacted with are defined during the design of both: the Simulink model and ControlDesk layout.

This layout was designed to allow enabling and disabling the boost converter, to turn on/of the MPPT algorithm implemented, in this case the P&O Algorithm from Figure 2.11, as well as the step of the algorithm. Furthermore, It is also possible to adjust the PI gains CCBC, and set the the parameters for an additional layer of overvoltage protection.

The IGBTs switches housed in the PM7575RLA120 power module from Mitsubishi Electric [55] are controlled via the BP7B isolation circuit from Powerex [56].

Figure 3.17 shows the experimental setup, associating each block from Figure 3.15 to its respective component in the physical setup, and Figure 3.18 shows a better view of the motor and the generator.

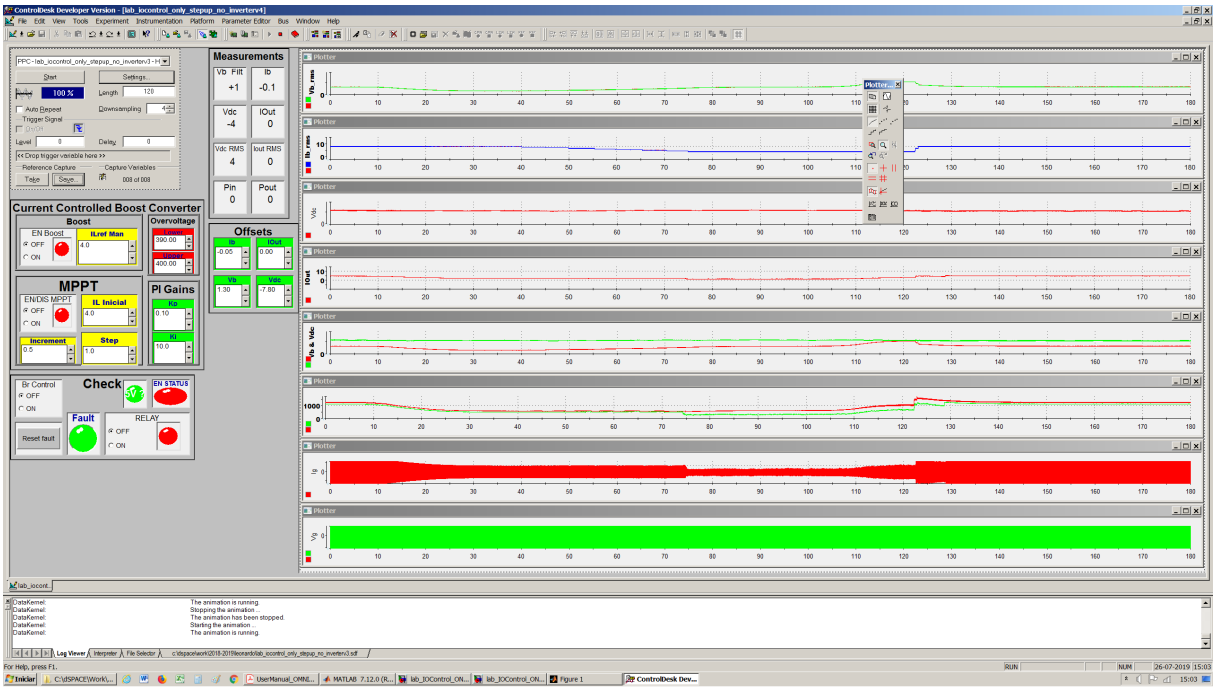

Figure 3.16: dSPACE ControlDesk Interface [54].

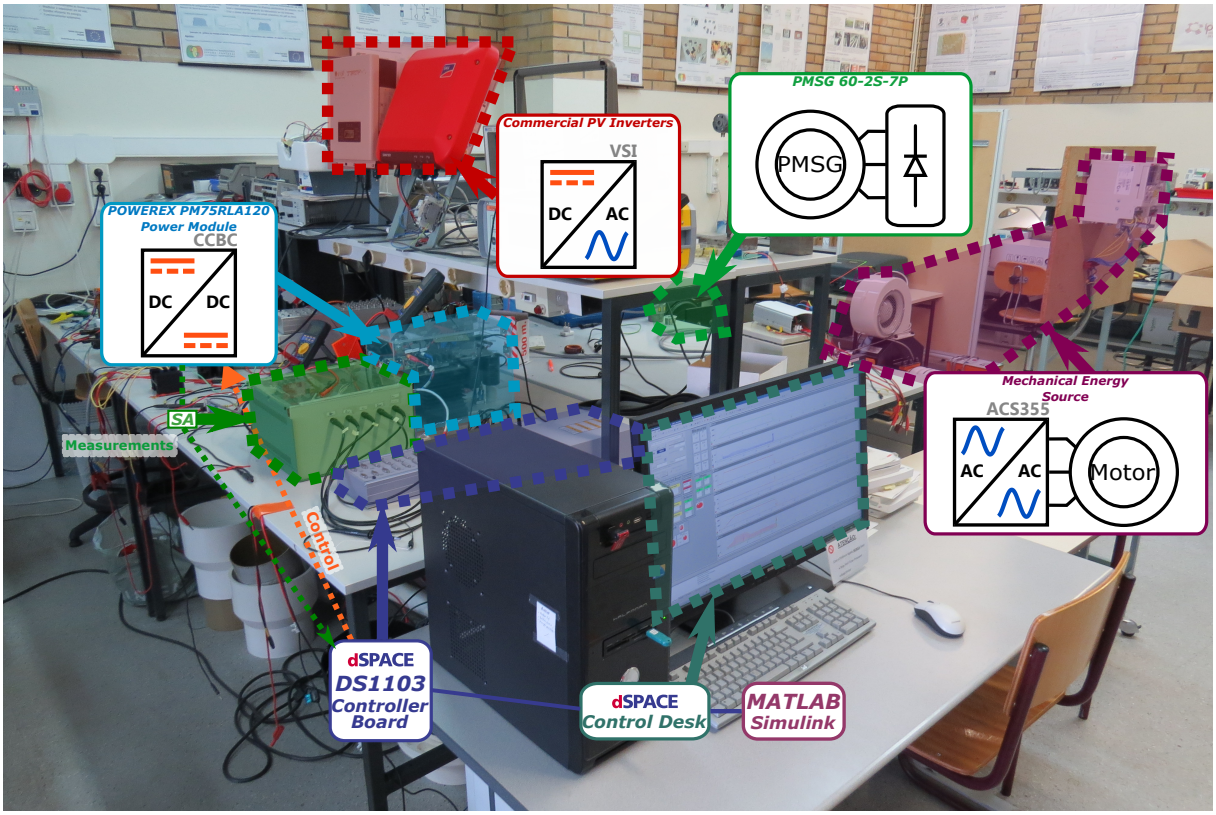

Figure 3.17: Experimental setup overview.

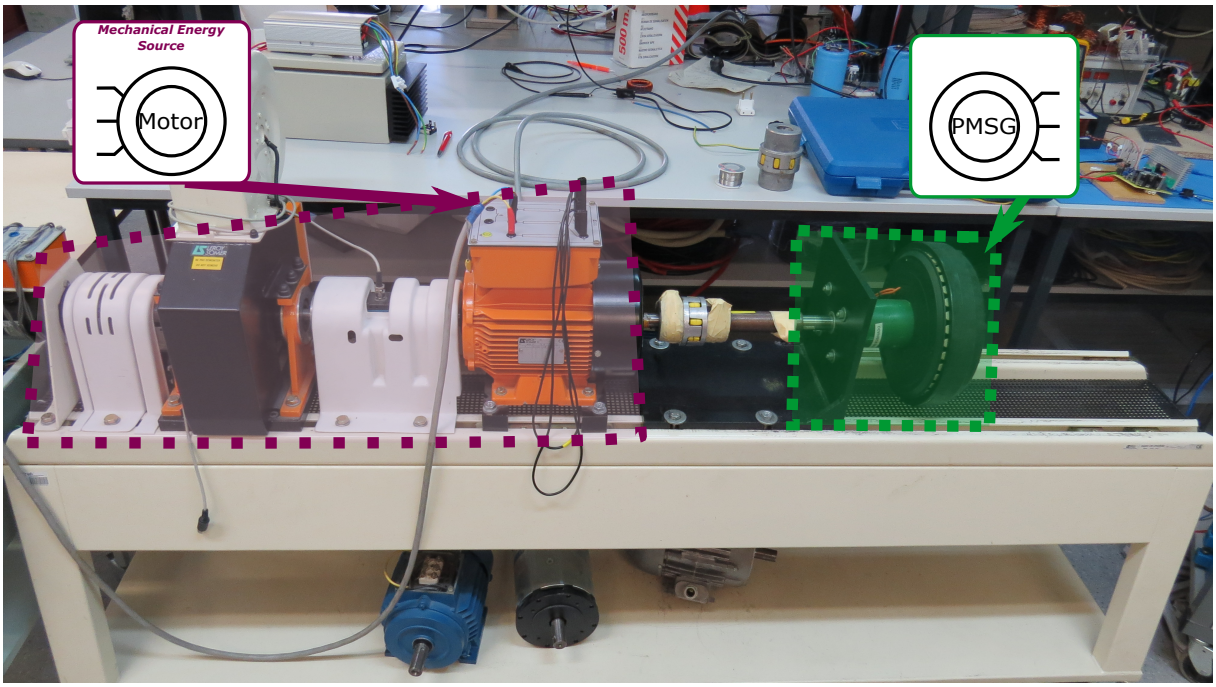

Figure 3.18: Motor and generator.

Chapter 4

Results and Discussion

This Chapter presents the results from all tests made. It is divided into three sections: Simulation Results, Experimental Results and Discussion and Analysis.

4.1 Simulation Results

This section contains the results obtained via simulation with the computational implementation of the power systems under study. The results shown in this chapter are discussed in the Discussion Section.

The experiments were done for the PV inverter emulation tested in Hardware-in-the-Loop (HIL) in [19]. It is important to note that, for all Software-in-the-Loop (SIL) tests, the Voltage Source Inverter (VSI) was disabled before the first second mark, and all oscillations and high values that may appear are due to the transient states of the simulation.

- Test 1, simulation only contains the generator with an emulation of an inverter;
- Test 2, the Current-Controlled Boost Converter (CCBC) as the power interface between the rectified generator and the VSI;
- Test 3, the Current-Controlled Ćuk Converter (CCCC) as the power interface between the rectified generator and the VSI.

4.1.1 Test 1

Figures 4.1 through 4.5 show the results collected when setting the mechanical power to 1422 W. The PV inverter emulation is enabled from 1 s. For each Commercial Phtovoltaic Inverter (CPVI), first is shown the input voltage and current then its respective output voltage and current.

Figures 4.3 and 4.4 shows a zoom of the transitions from the Figure 4.2, periods 1 s-3 s and 5 s-6 s, respectively. In them, It's show that the inject current is in phase with the grid voltage.

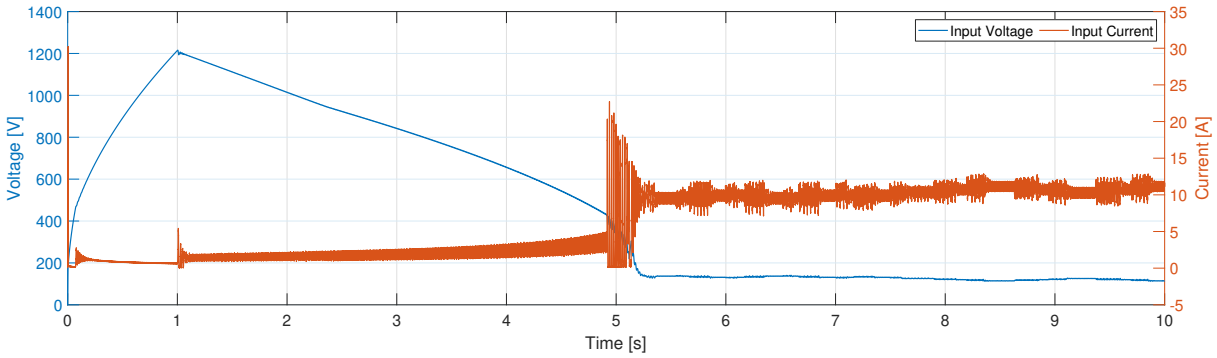

Figure 4.1: Input voltage and current for the PV inverter emulation.

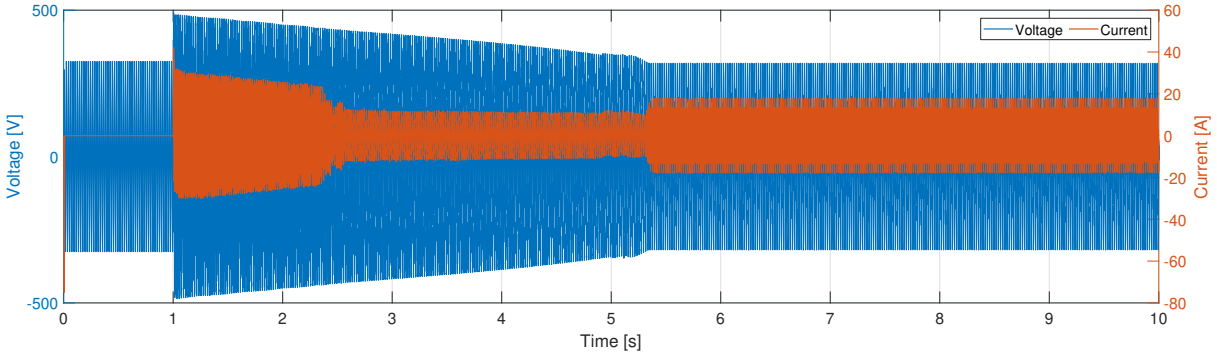

Figure 4.2: Grid voltage and injected current.

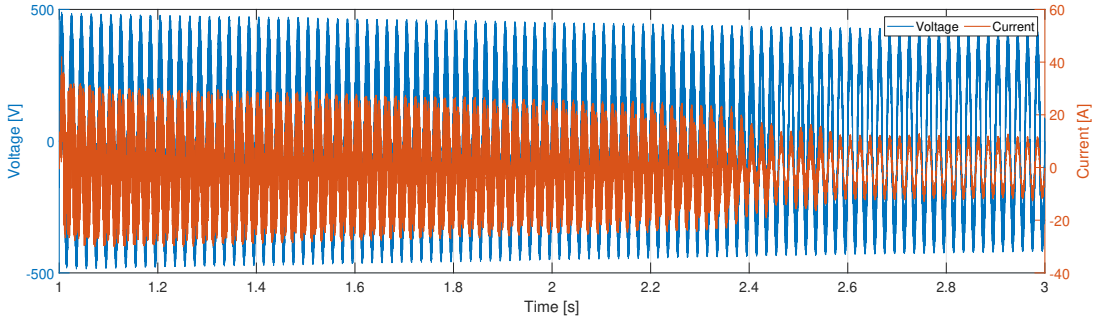

Figure 4.3: Grid voltage and injected current from 1 s to 3 s.

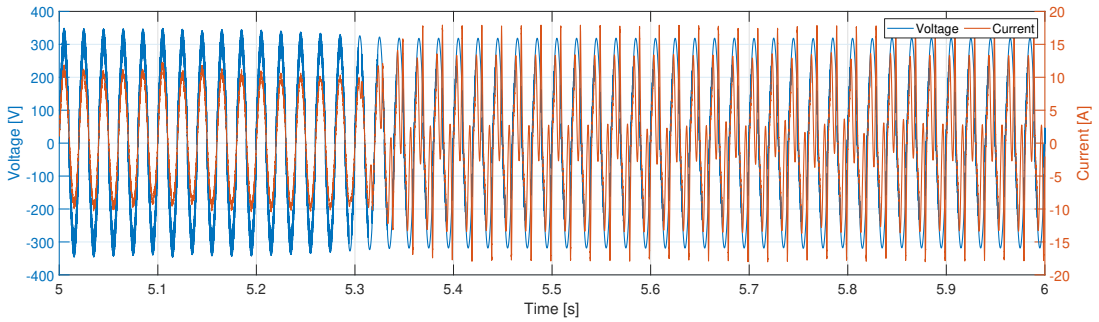

Figure 4.4: Grid voltage and injected current from 5 s to 6 s.

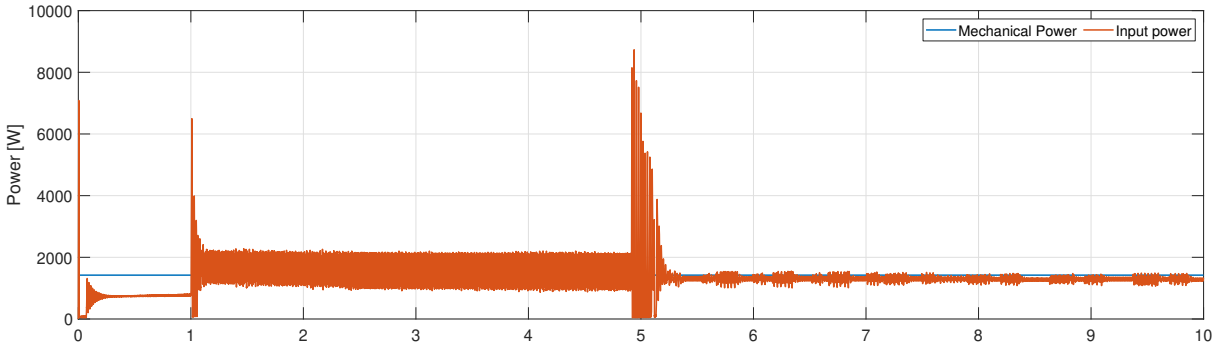

Figure 4.5: Mechanical input power and VSI's input power.

Observing Fig. 4.8 it is possible to note that, after being turned on, at 1 s, the system reaches Steady-State after the 5 s mark, when the grid voltage and the injected current stabilizes and are synchronized with the grid, Figure 4.4, which means that the PV inverter emulation is working well.

4.1.2 Test 2

Figures 4.6 through 4.9 show the results collected when setting the mechanical power to 1422 W. The PV inverter emulation is enabled from 1 s and the set-point, I_{ref} is being varied, to explore the power curve extracted from the generator. Figure 4.6, the current does not follow the reference I_{ref}, that means that the PV inverter emulation is bypassing the boost converter and directly enforcing the operation point of the generator.

In Fig. 4.8, where the injected current and grid voltage are shown, it is important to note that the system is stable from 2.5 s to 7.75 while for other instants, the grid voltage amplitude is not

equal to 325 V.

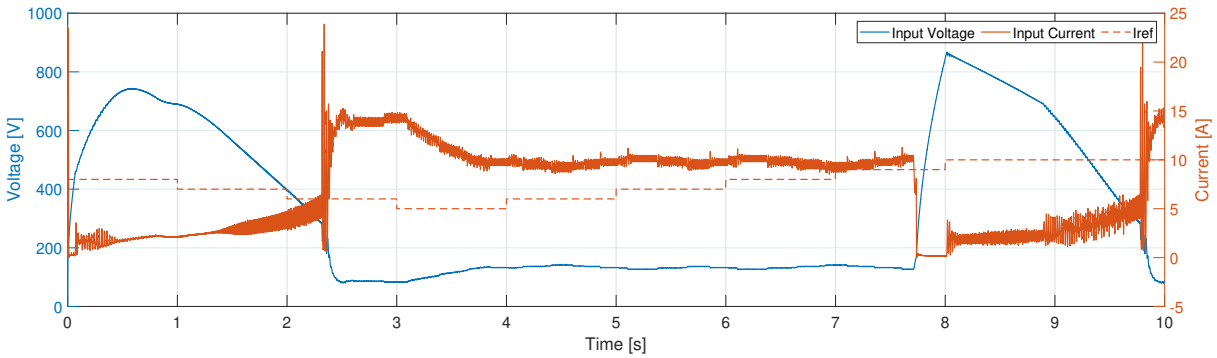

Figure 4.6: Input voltage and current for the CCBC.

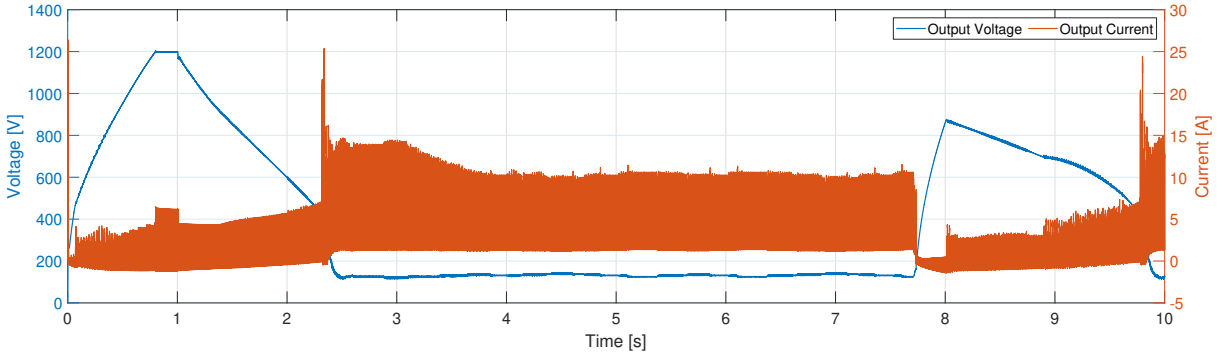

Figure 4.7: Output voltage and current for the CCBC.

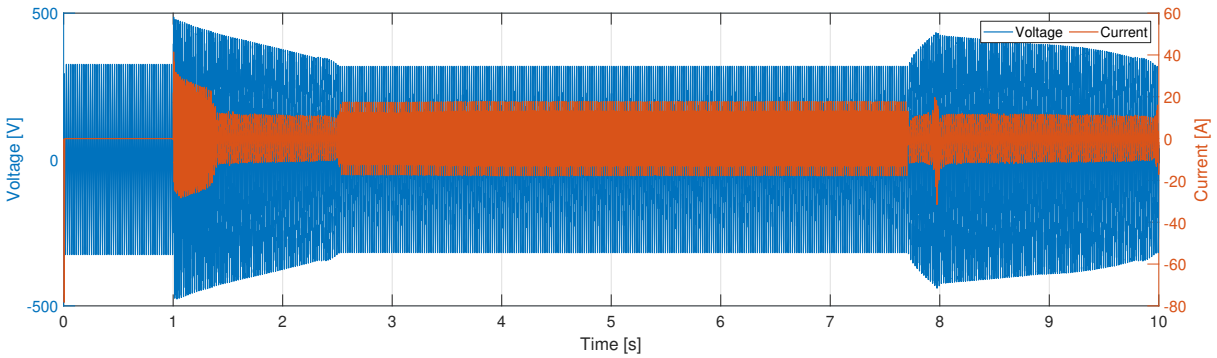

Figure 4.8: Voltage and injected current.

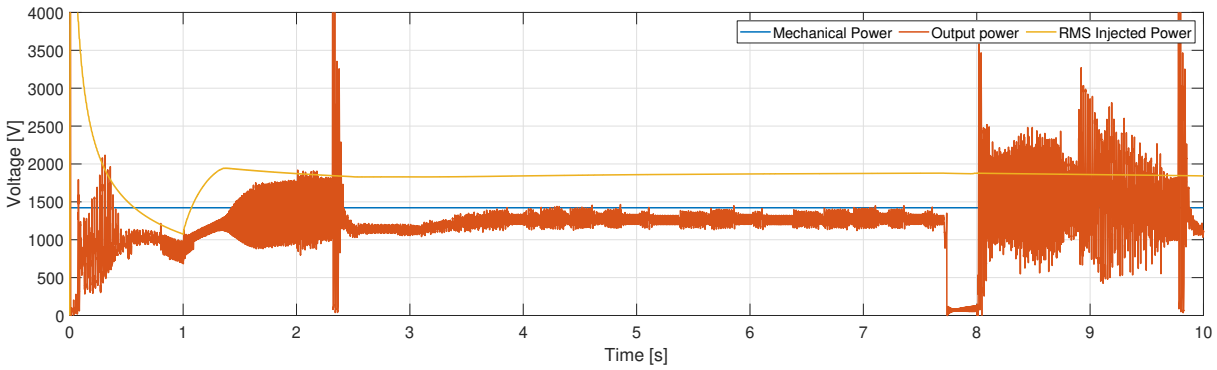

Figure 4.9: Mechanical input power and CCBC's output power.

4.1.3 Test 3

Figures 4.10 through 4.12 show the results collected when setting the mechanical power to 1422 W. The PV inverter emulation is enabled from 1 s and the set-point, hence the existence of transients. The set-point I_{ref} is being varied, to explore the power curve extracted from the generator.

In Figure 4.10, the controller is enforcing the input current, as it was designed to, and the generator is working as a current source, but when comparing with Figure 4.11, the voltage values are similar, so the PV inverter emulation is still controlling the voltage. Figure 4.12 shows the power being supplied to as input into the system, as well as the power being extracted by the CCCC.

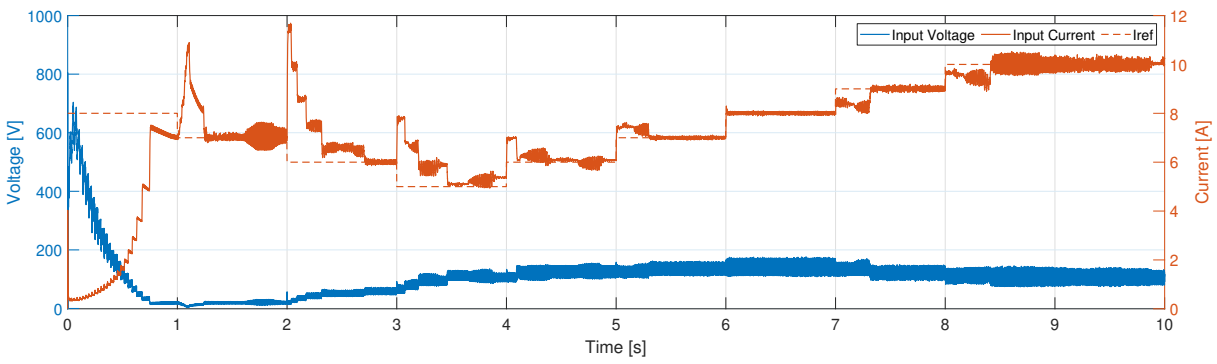

Figure 4.10: Input voltage and current for the CCCC.

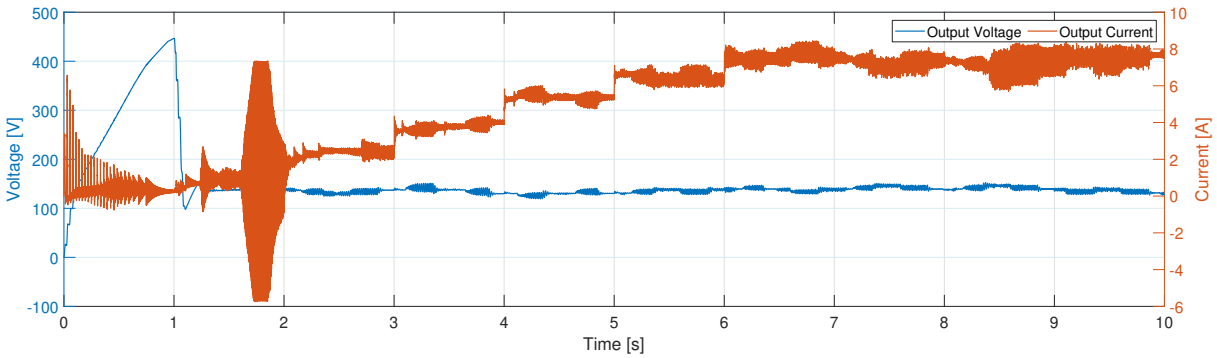

Figure 4.11: Output voltage and current for the CCCC.

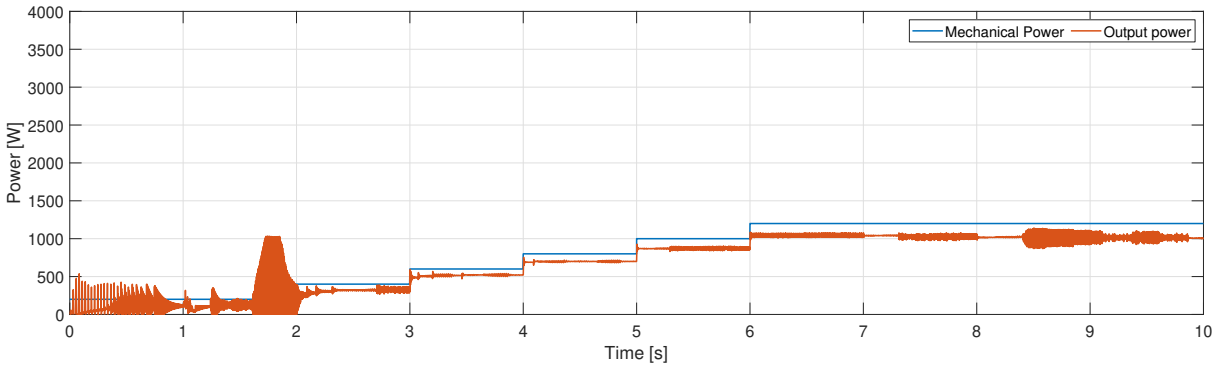

Figure 4.12: Mechanical input power and CCCC's output power.

4.2 Experimental Results

This section contains the results obtained via experimentation with the physical implementation of the power system under study. The results shown in this chapter are discussed in Analysis Section.

The experiments were done for the four CPVI found in Table 2.2. They are the Omniksol-2k-TL2, the Kostal Piko MP Plus 1.5-1, the SB 2100TL, and the Solax X1-1.5-S-D. All CPVI are put under the four tests:

- Test 1, the power reference set in the ABB ACS355 was 1000 W, with varying current references;
- Test 2, the power reference set in the ABB ACS355 was 1200 W, with varying current references;

- Test 3, the power reference set in the ABB ACS355 was 1300 W, with varying current references;
- Test 4: the power reference set in the ABB ACS355 was 1600 W, with varying current references.

4.2.1 Test 1

Figures 4.13 through 4.20 show collected when setting the power reference in the ABB ACS355 to 1000 W. For each CPVI, first is shown the input voltage and current then its respective output voltage and current.

Figures 4.13, 4.15, and 4.19 shows the input current being set by the CCBC's controller, while the input voltage is similar to what is shown in their respective output counterparts, Figures 4.14, 4.16, and 4.20. The exception are Figures 4.17 and 4.18, which the input operation voltage is independent from the output.

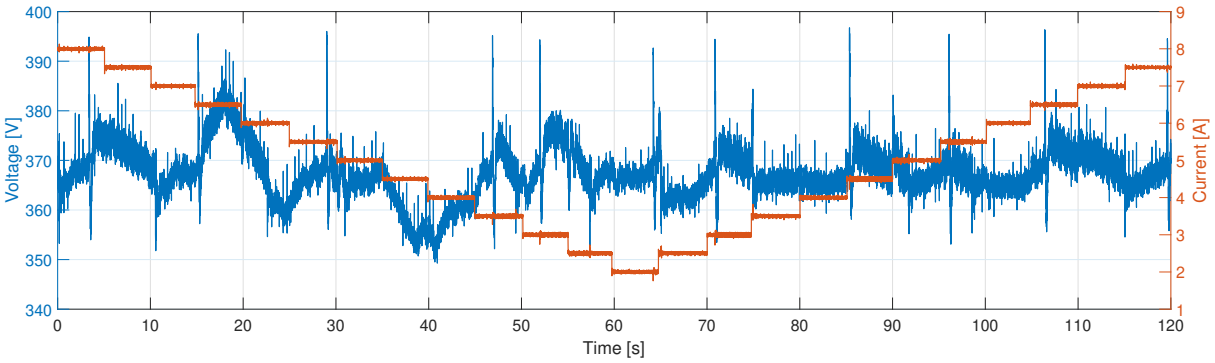

Figure 4.13: Input voltage and current for the Ominiksol-2k-TL2 CPVI.

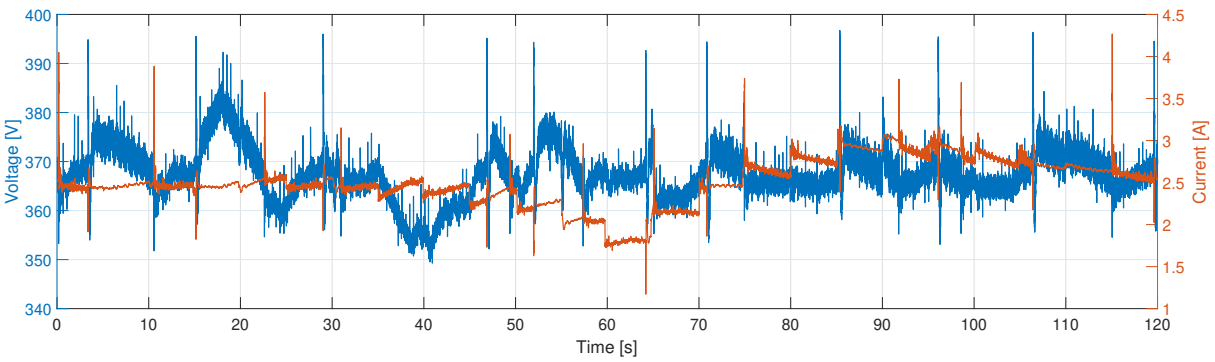

Figure 4.14: Output voltage and current for the Ominiksol-2k-TL2 CPVI.

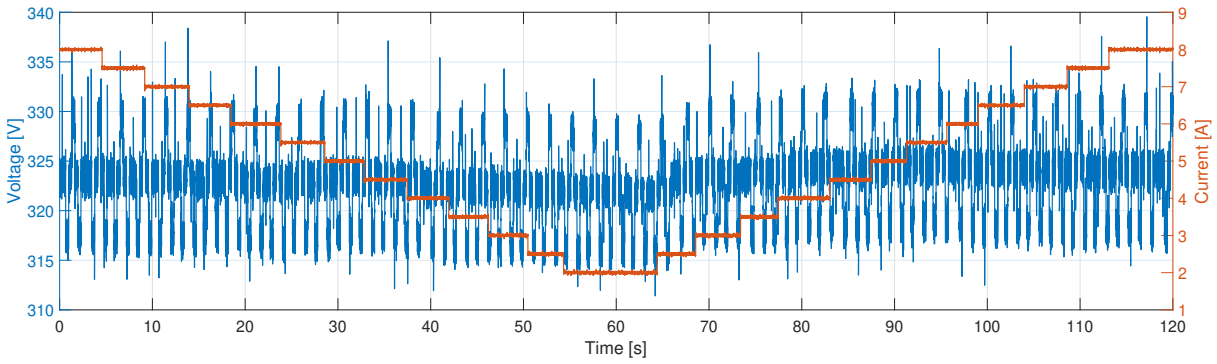

Figure 4.15: Input voltage and current for the Kostal Piko CPVI.

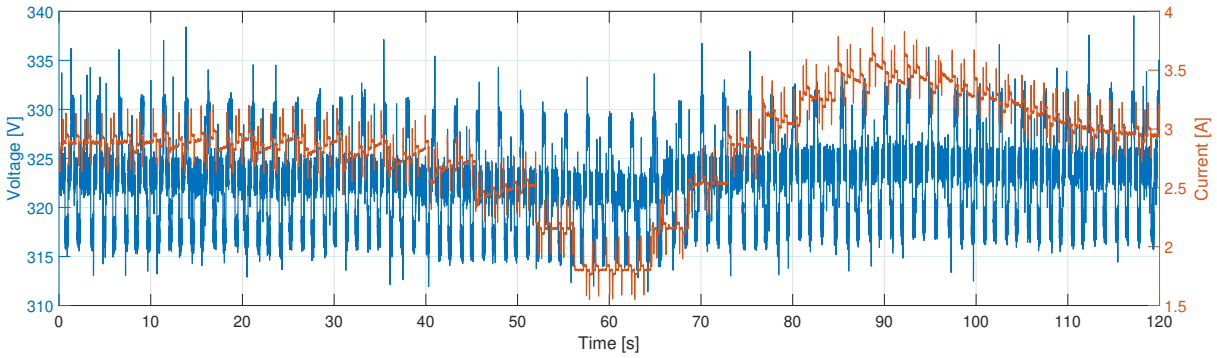

Figure 4.16: Output voltage and current for the Kostal Piko CPVI.

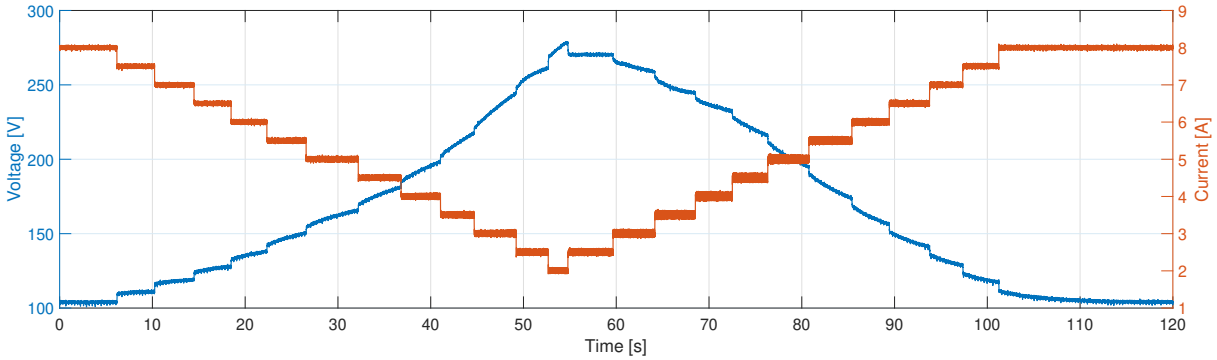

Figure 4.17: Input voltage and current for the SB 2100TL CPVI.

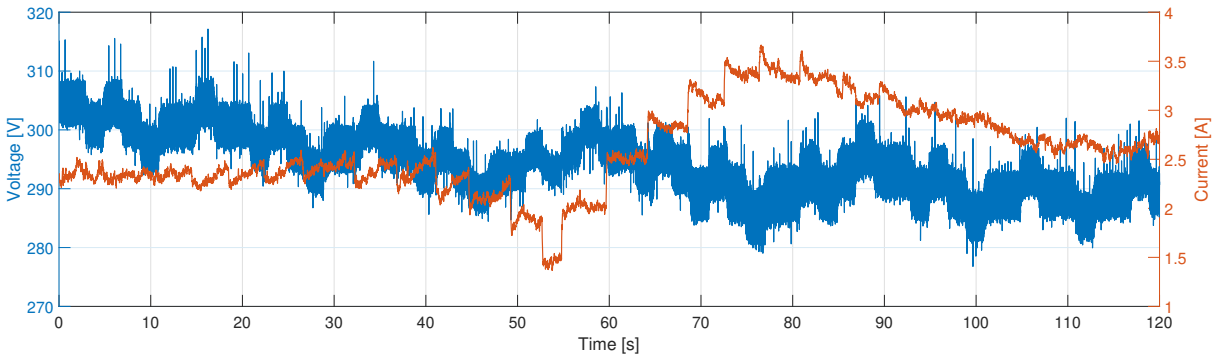

Figure 4.18: Output voltage and current for the SB 2100TL CPVI.

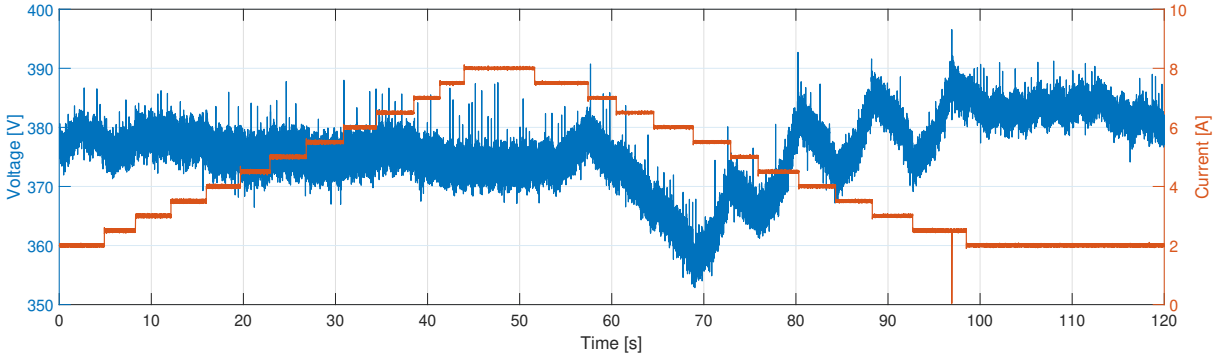

Figure 4.19: Input voltage and current for the Solax X1-1.5-S-D CPVI.

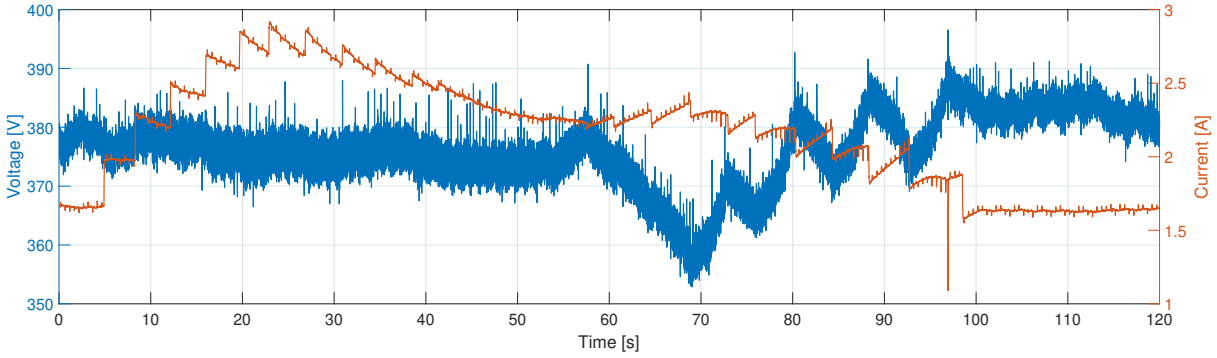

Figure 4.20: Input voltage and current for the Solax X1-1.5-S-D CPVI.

4.2.2 Test 2

Figures 4.21 through 4.28 show collected when setting the power reference in the ABB ACS355 to 1200 W. For each CPVI, first is shown the input voltage and current then its respective output voltage and current.

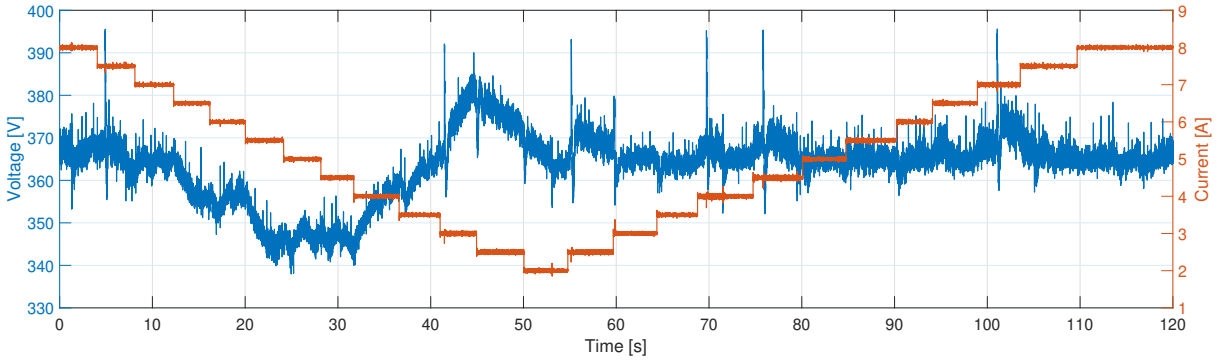

Figure 4.21: Input voltage and current for the Ominiksol-2k-TL2 CPVI.

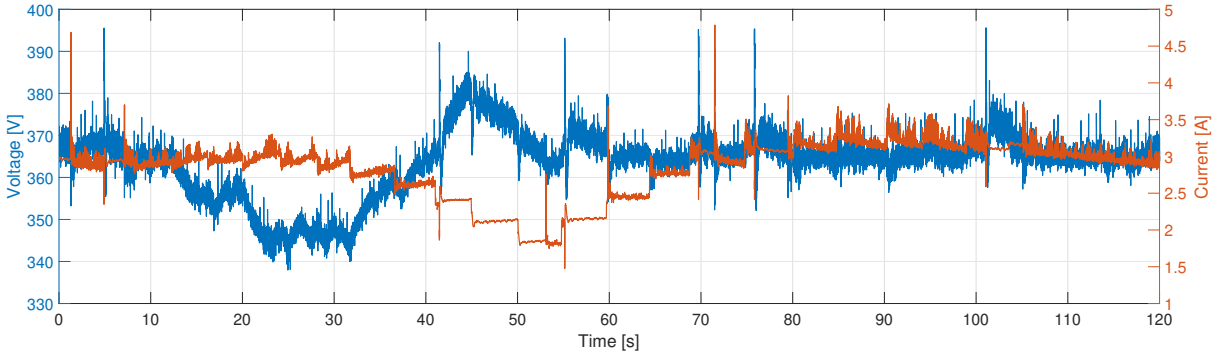

Figure 4.22: Output voltage and current for the Ominiksol-2k-TL2 CPVI.

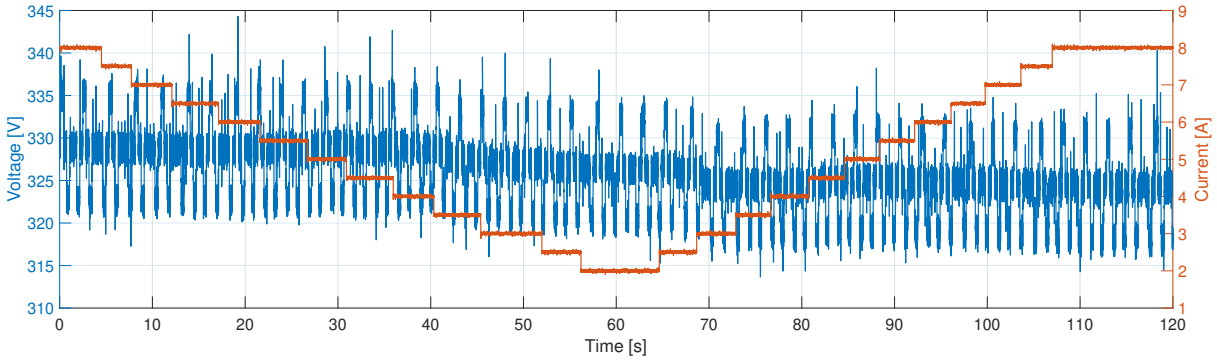

Figure 4.23: Input voltage and current for the Kostal Piko MP Plus CPVI.

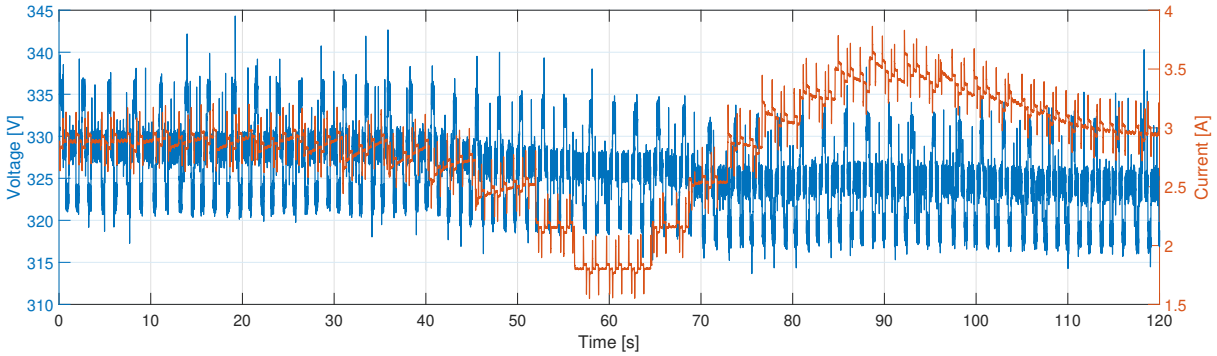

Figure 4.24: Output voltage and current for the Kostal Piko MP Plus CPVI.

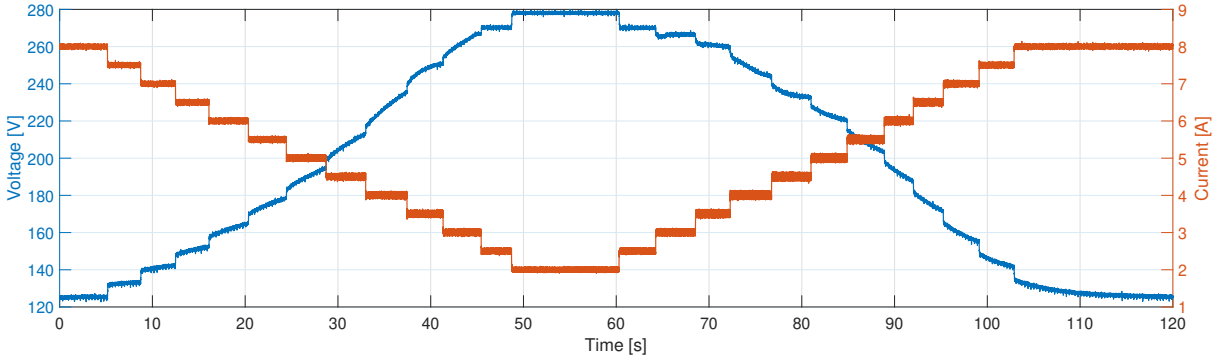

Figure 4.25: Input voltage and current for the SB 2100TL CPVI.

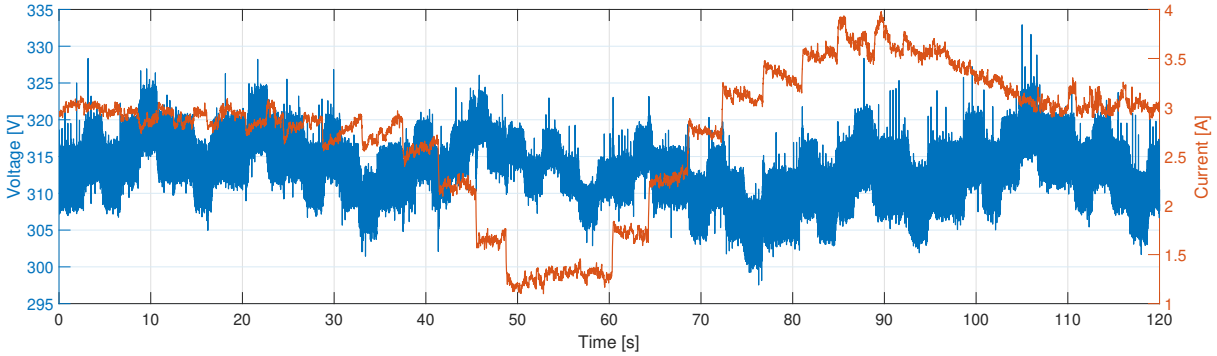

Figure 4.26: Output voltage and current for the SB 2100TL CPVI.

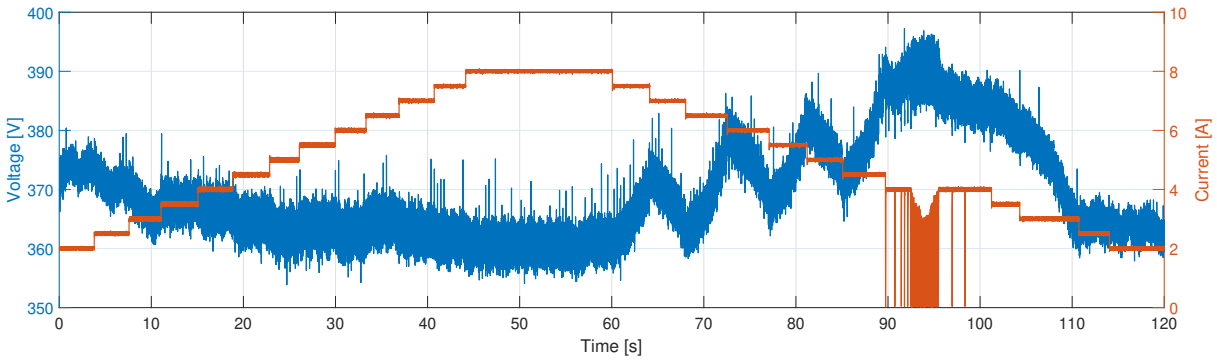

Figure 4.27: Input voltage and current for the Solax X1-1.5-S-D CPVI.

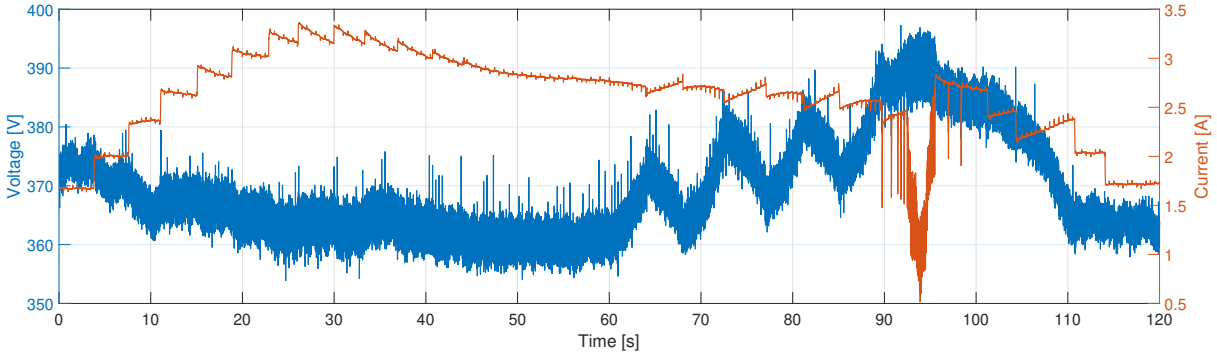

Figure 4.28: Input voltage and current for the Solax X1-1.5-S-D CPVI.

4.2.3 Test 3

Figures 4.29 through 4.36 show collected when setting the power reference in the ABB ACS355 to 1300 W. For each CPVI, first is shown the input voltage and current, then its respective output voltage and current.

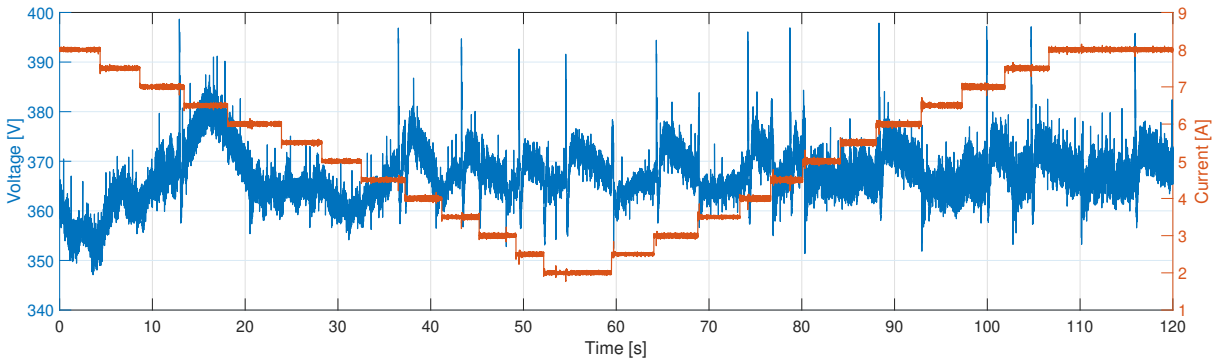

Figure 4.29: Input voltage and current for the Ominiksol-2k-TL2 CPVI.

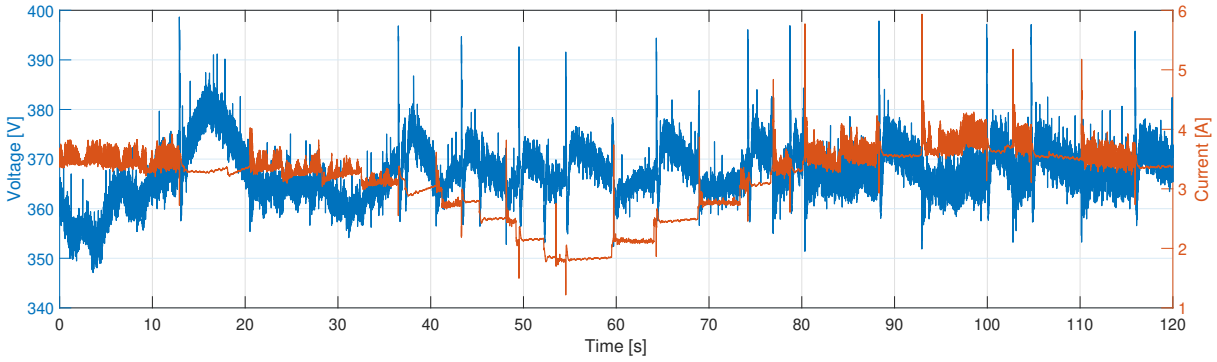

Figure 4.30: Output voltage and current for the Ominiksol-2k-TL2 CPVI.

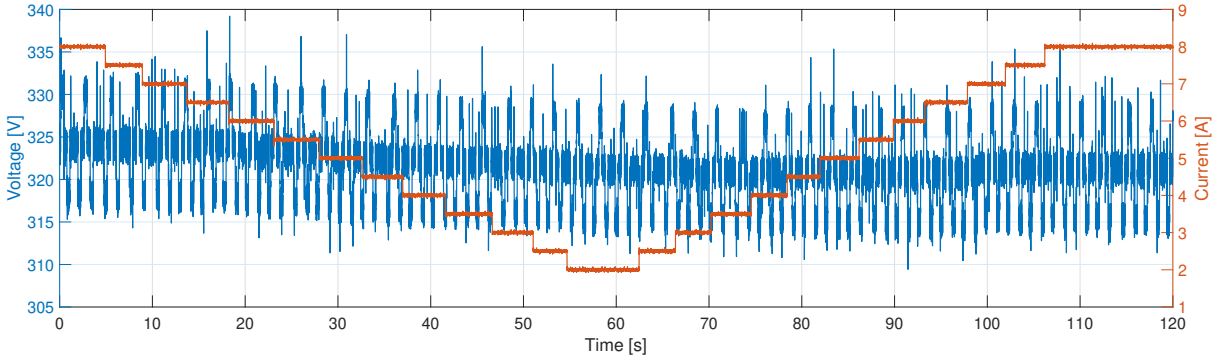

Figure 4.31: Input voltage and current for the Kostal Piko MP Plus CPVI.

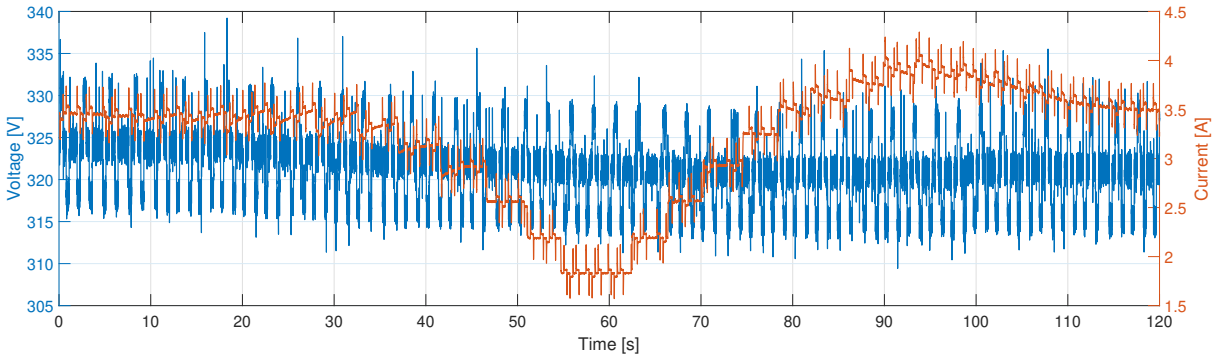

Figure 4.32: Output voltage and current for the Kostal Piko MP Plus CPVI.

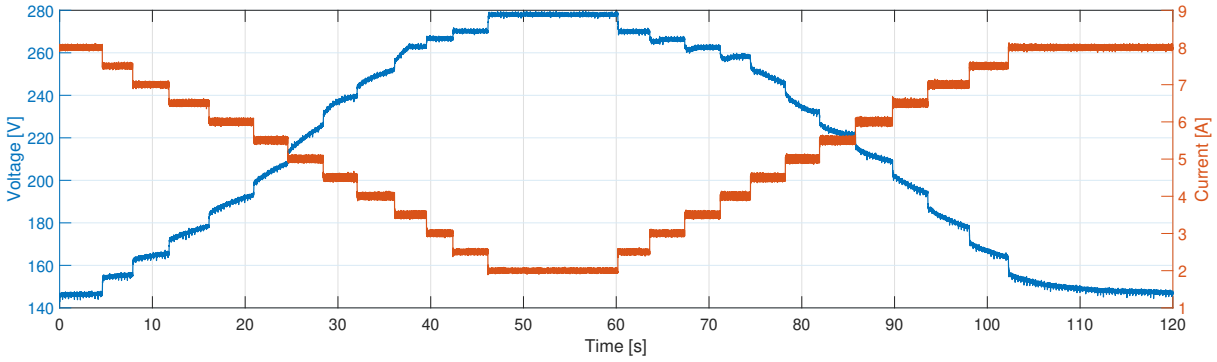

Figure 4.33: Input voltage and current for the SB 2100TL CPVI.

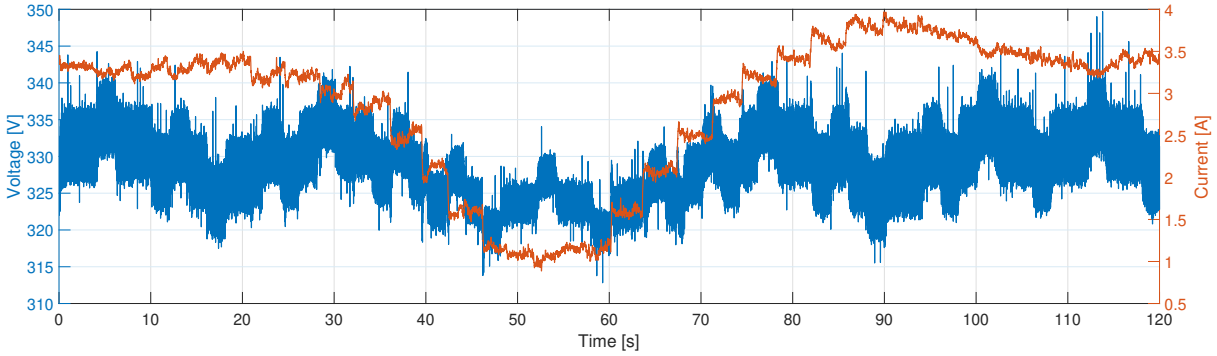

Figure 4.34: Output voltage and current for the SB 2100TL CPVI.

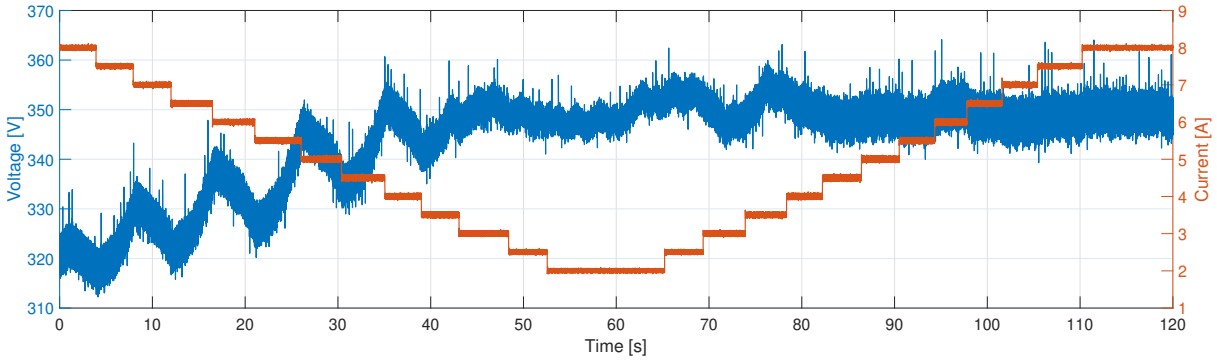

Figure 4.35: Input voltage and current for the Solax X1-1.5-S-D CPVI.

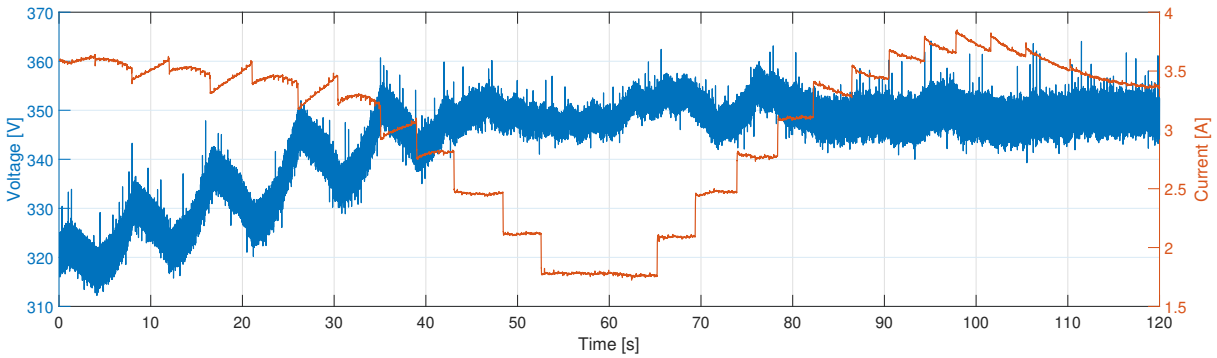

Figure 4.36: Input voltage and current for the Solax X1-1.5-S-D CPVI.

4.2.4 Test 4

Figures 4.37 through 4.44 show collected when setting the power reference in the ABB ACS355 to 1600 W. For each CPVI, first is shown the input voltage and current then its respective output voltage and current.

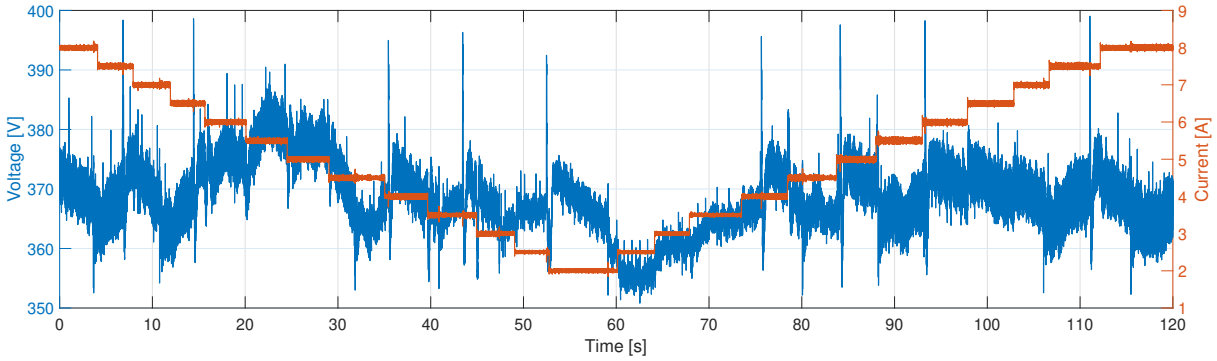

Figure 4.37: Input voltage and current for the Ominiksol-2k-TL2 CPVI.

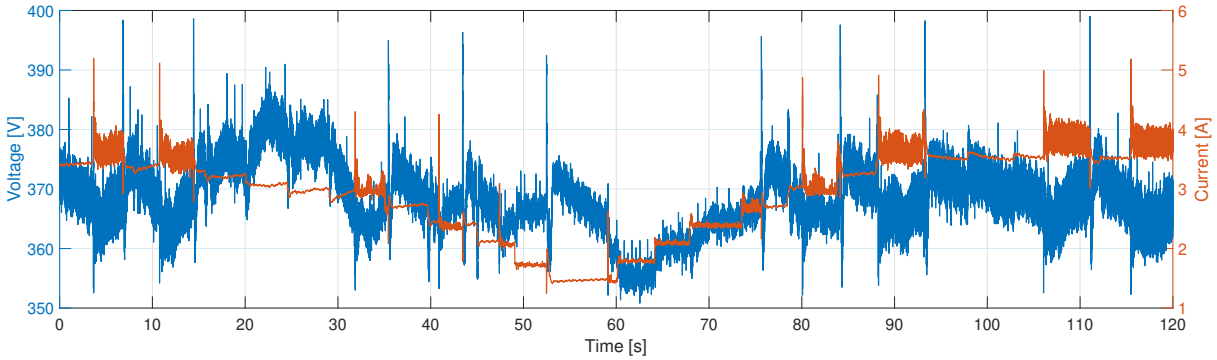

Figure 4.38: Output voltage and current for the Ominiksol-2k-TL2 CPVI.

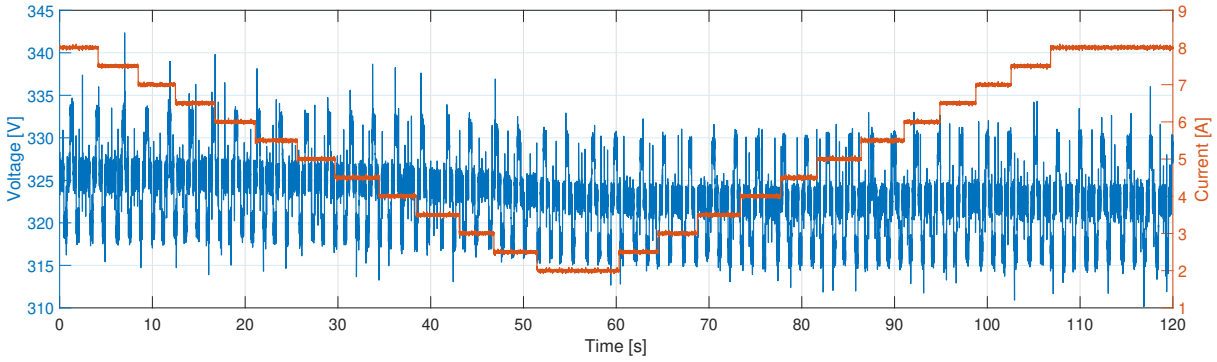

Figure 4.39: Input voltage and current for the Kostal Piko MP Plus CPVI.

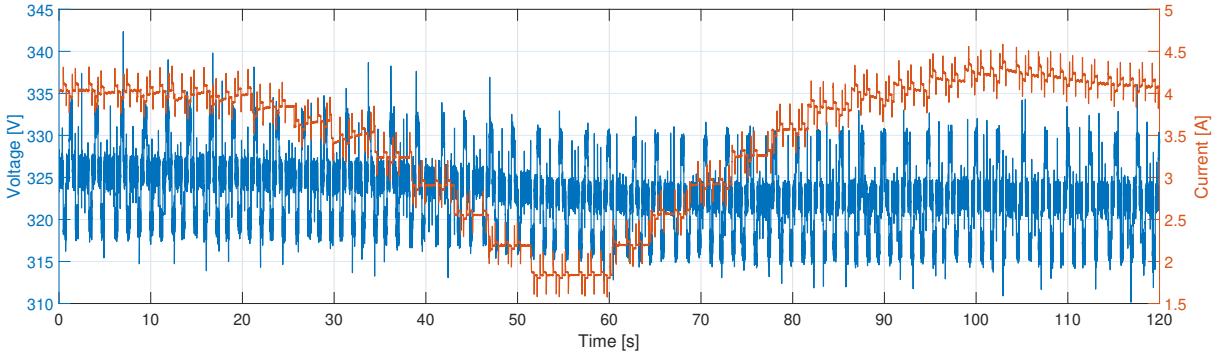

Figure 4.40: Output voltage and current for the Kostal Piko MP Plus CPVI.

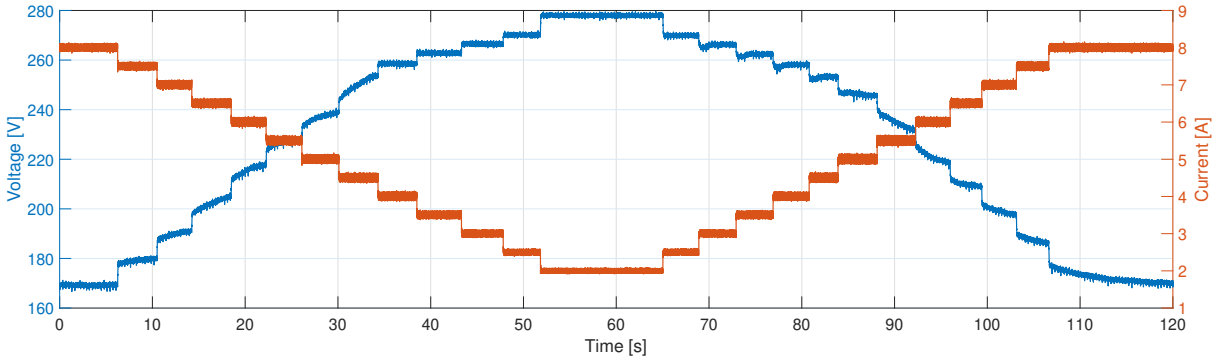

Figure 4.41: Input voltage and current for the SB 2100TL CPVI.

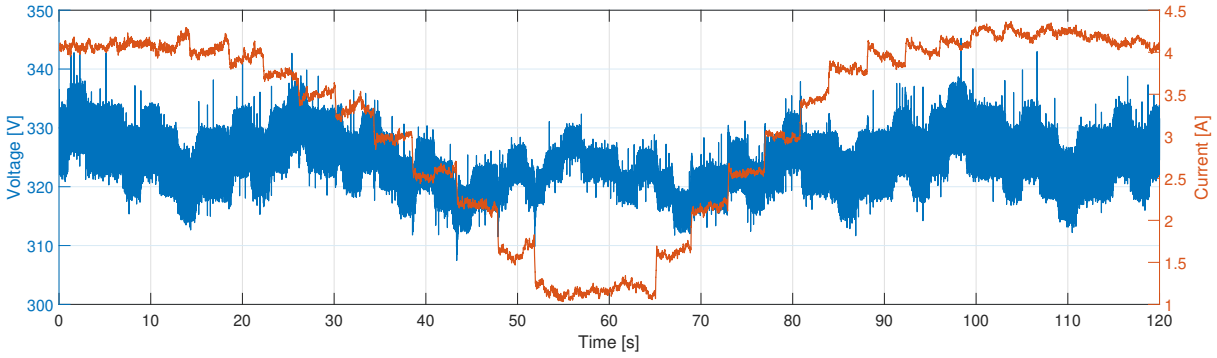

Figure 4.42: Output voltage and current for the SB 2100TL CPVI.

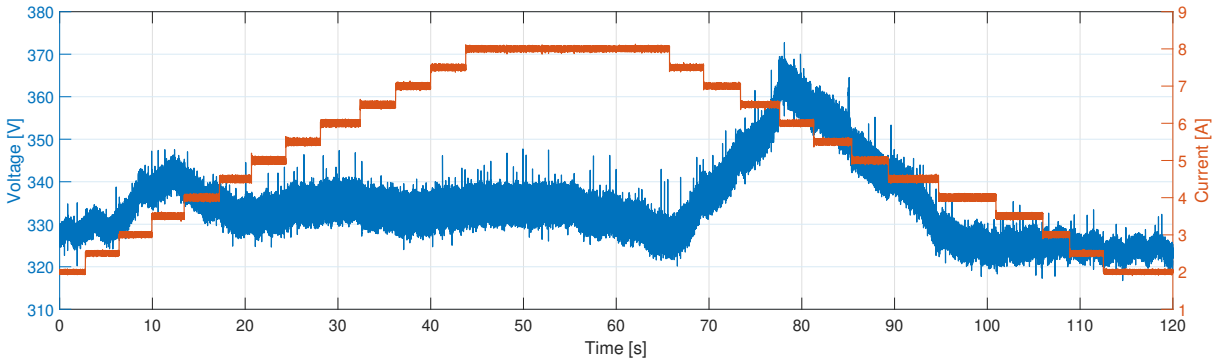

Figure 4.43: Input voltage and current for the Solax X1-1.5-S-D CPVI.

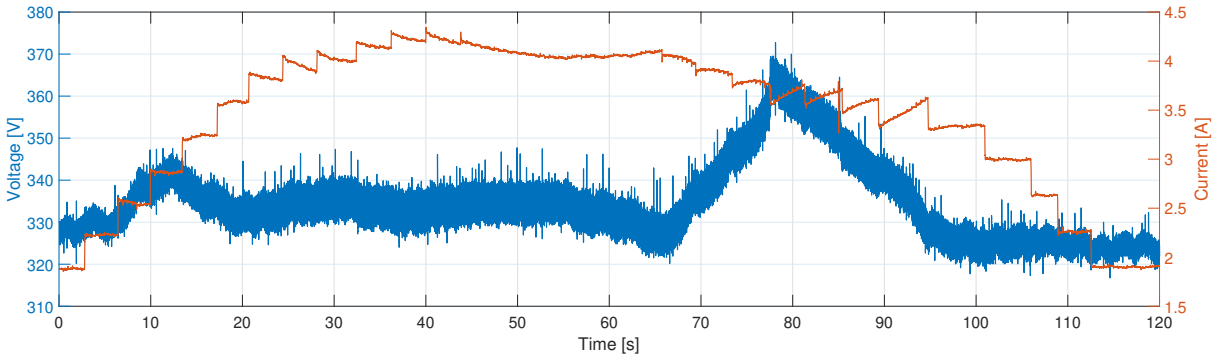

Figure 4.44: Output voltage and current for the Solax X1-1.5-S-D CPVI.

4.2.5 Voltage-Current Curves

The data acquired during the tests were manipulated through the Script A.1 to average the values at the closest point to the steady-state condition. The script analyzes the data for the input current,

searching for abrupt changes, using the Matlab ischange function [57], which return a vector of indices that point where they happen. Then these indexes are used as the indices for the mean function, which calculates the averages between the index and its preceding 625 data points. This was done for input and output voltages and currents.

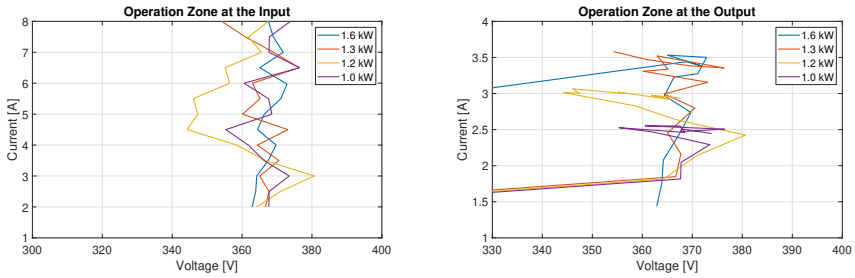

Figure 4.45: Voltage-Current curve using the averaged data of Figure A.1 for Ominiksol-2k-TL2 CPVI.

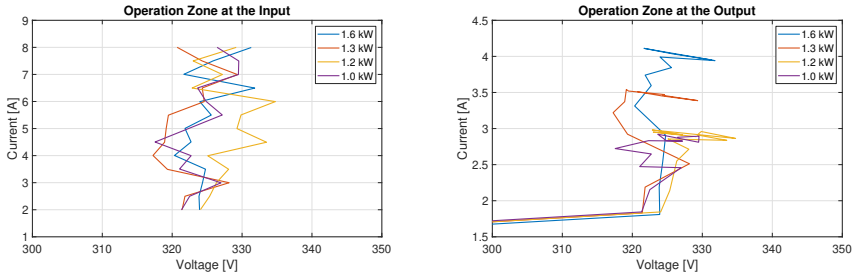

Figure 4.46: Voltage-Current curve using the averaged data of Figure A.2 for Kostal Piko MP Plus CPVI.

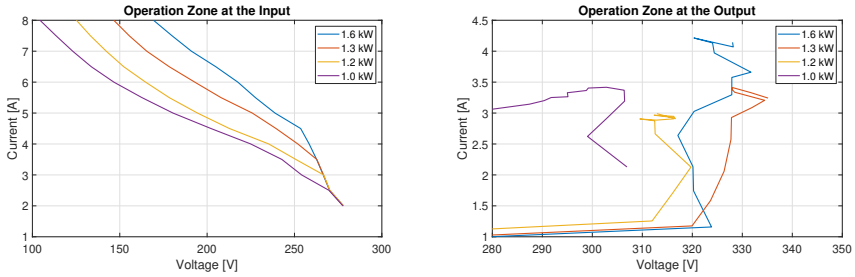

Figure 4.47: Voltage-Current curve using the averaged data of Figure A.3 for SB 2100TL CPVI.

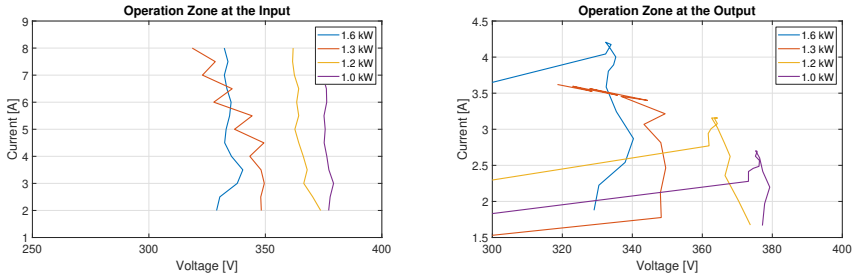

Figure 4.48: Voltage-Current curve using the averaged data of Figure A.4 for Solax X1-1.5-S-D CPVI.

4.2.6 Incident

During the execution of the 1600W Test for the Omniksol-2k-TL2, there was an incident; the fault light indication was lit up in the ControlDesk. As a default protection, the CCBC was disabled, although the system kept operating. Basically, the V_B voltage direct polarized the Diode of the Insulated-gate Bipolar Transistor (IGBT) switch S_1, thus bypassing the CCBC. Hence, Omniksol kept operating, and its Maximum Power Point Tracking (MPPT) algorithm kept reducing the DC Bus voltage. Thus it was brought close to the inferior limit of the range for this PV inverter, as seen in Figure 4.49.

The Fault function does not allow the power structure to be switched on/off until it has been reset, through the "Reset fault" button in the ControlDesk, shown in Figure 3.16 - where a red light means a fault has happened and the green light means that no fault has occurred. So, after resetting the Fault, the CCBC was not able to restart operating by making its input and output operate in different operating zones.

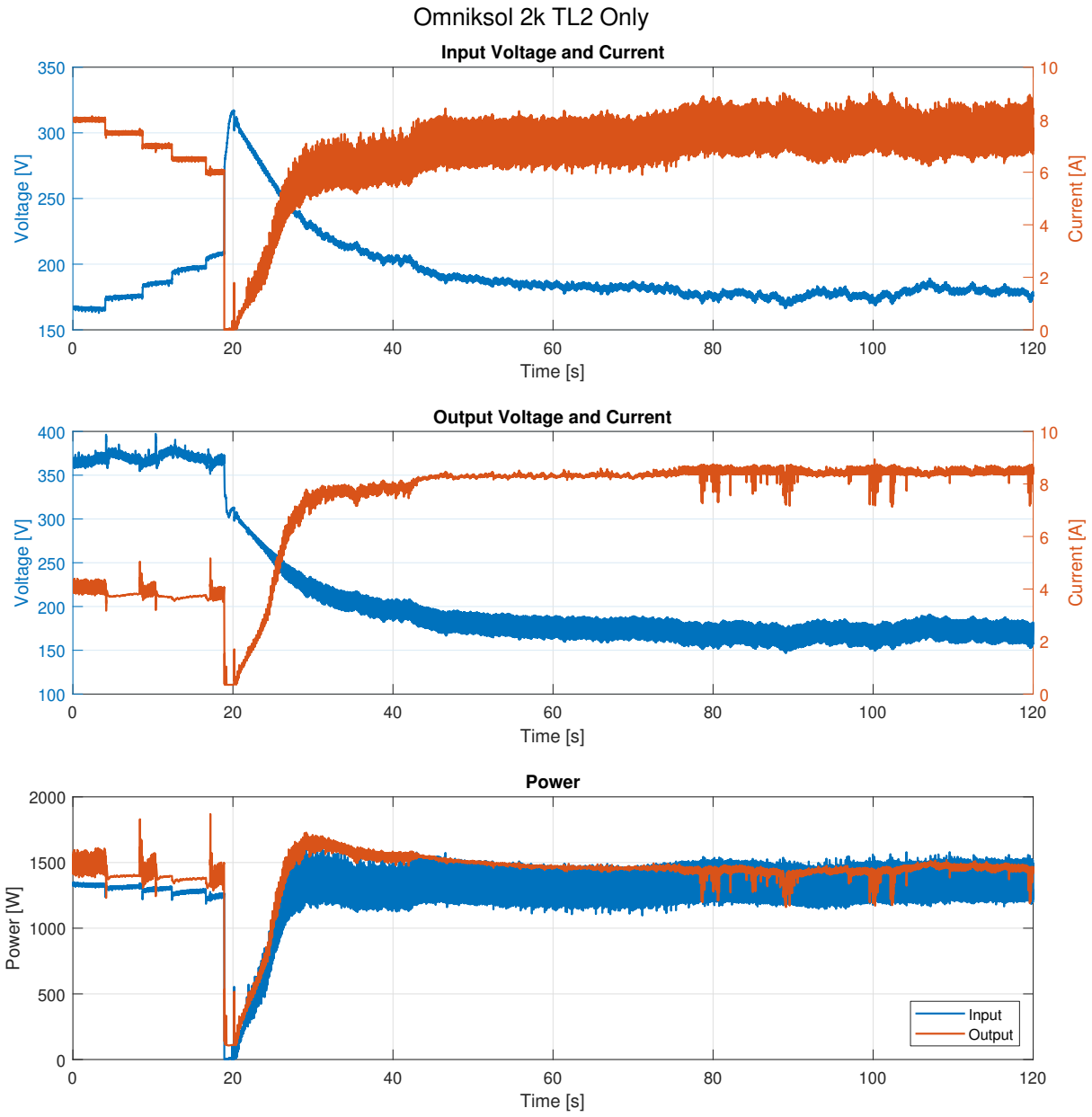

Figure 4.49: The Fault happened at 19 s, and CCBC stopped working

4.3 Discussion and Analysis

This sections presents the discussion and analysis of the results shown in previous sections.

From Figures 4.10 through 4.12, it can be seen that the CCCC's controller worked better for certain set-points, but overall, it was able to make the Permanent Magnet Synchronous Generator (PMSG)'s operation current independent from the PV inverter, as it was able to limit the input

current to the nominal value (8 A), although the operation voltage was still set by the PV inverter emulation. Furthermore, it was able to define the amount of power being extracted from the generator without being bypassed by the pv inverter emulation.

The results obtained from the SIL's Test 2, were somewhat similar to what happened in Figure 4.49, after the 20 s mark. The PV inverter emulation is defining the voltage at the output to a lower value than the value at the input, i.e., for both of them, the boost is being bypassed, and the controller is neither controlling the input current nor the operation point of the PV inverter.

Even though the CCBC's results were not as expected, the HIL tests shows that it is indeed a feasible solution. This suggests that there are some issues with the PV inverter emulation used, and that it can still be improved.

Similarly, another important lesson taken from the HIL test, for the CCBC, is the necessity of adding minimum difference between the input and output voltages; otherwise, the CPVI is going to bypass the boost converter, rendering it useless.

From the results obtained during HIL experiments shown in Figures 4.14 through 4.44, it can be noted that the designed PI controller of the CCBC was able to define the input current for every case, even more so, it was able to work independently from whatever voltage set-point by the PV inverter.

The data collected for the testes made with the SB 2100 TL CPVI, e.g., Figure 4.17, are the ones that better corresponded with what this thesis aims for. As the input current drops, the voltage increases, as the mechanical power supplied to the generator remains constant throughout the same test. Another essential detail is the fact that the time for the voltage to reach the steady-state increases as the current drops, so further tests are made necessary, to investigate the behavior of the Maximum Power Point (MPP) for each input power.

Another important detail is related to the Solax X1-1.5-S-D CPVI, Figures 4.19, 4.20, 4.27, and 4.28, these tests presents a sudden current drop, in the latter half of the test, when the current reference is being lowered, on the other hand, the voltage rises. Contrary to all that, Figures 4.35, 4.36, 4.43, and 4.44 show no such behavior. So, it can be inferred that the MPPT algorithm of this CPVI judges it is necessary to measure the Open Circuit Voltage at those points, but as each manufacturer has its own MPPT algorithm and they do not share details on it, this makes it more

difficult to predict this type of behavior [40].

Analyzing the data summarized in the Voltage-Current Curves shown in Figures 4.45 through 4.48, and the efficiency curves from each of their manuals, the CPVIs are working in the voltage in which they work close to their highest efficiencies. Hence, after noticing this tendency happening in the HIL, it is necessary to take it into account for the CPVI emulation being done in the SIL, as to represent better the commercial device, which will further improve the researchers ability to predict e detect possible design issues. A solution for this is to implement an efficiency curve, taken from a CPVI, artificially, so that its MPPT algorithm will tend to work in regions with better efficiency.

In Summary, the CCBC tested in the hardware platform, were able to make the Permanent Magnet Alternator (PMA)'s operation point independent of what was being set by the PV inverter, which had its MPPT working normally, as the power is constant throughout the system. The tested solutions works by coupling both of them through a power interface, but at the same time, making them compatible with each other, enabling the generator to operate at its nominal current and the CPVI at its nominal voltage. Although further data is necessary for an efficiency analysis, as to aloow further statements on the overall power efficiency of this system, for now, it is possible to state that the proposed solution is technically feasible, and there is still the need to further research into it.

Chapter 5

Conclusions

The implementation of a power interface between a pico-hydro and a Commercial Phototovoltaic Inverter was successful, based on the achieved computational and experimental results presented in this document. Tests were performed both in the simulation and with the experimental setup to test the system and its feasibility, probe its stability under different operation conditions and with varying power supply.

While the system did not prove to be fault-proof, but it showed some limitations that can be further improved in future experiments. Furthermore, it still showed the potential of this strategy of using a current-controlled power interface to make the Maximum Power Point Tracking of pico-hydro and wind turbines, enhancing the ability of the inverter emulation of exploiting these renewable energy sources.

The system was tested using a real-time controller board from dSPACE. This controller board allows for rapid control prototyping, and identifying further improvements needed, although, it does not reflect the actual implementation of such a system for commercial purposes. For commercial purposes, it has to be implemented with a micro-controller, in the case of a more sophisticated digital control strategy or it can also be implemented using widely available analog components, and implement analog logic plus a PWM generator, e.g., the Texas TL494, to provide the switching signal for the switches.

Experimental validation corroborates the potential of this strategy and, also, with the Cúk Converters topology proposed, using the same control algorithm, points elucidated some issues that were not predicted previously, allowing to work towards a more generic, feasible, robust power interface to connect a renewable energy source, pico-hydro, to a commercial photovoltaic inverter, thus reaching the main thesis objective.

5.1 Future Works

This section contains suggestions on future lines of research related to the topic at hand, with the objective of further improving and testing of the proposed power interface strategy between a pico-hydro generators and Commercial Photovoltaic Inverters.

- Experimental validation in the steady-state condition for different current references.
- Implement a minimal difference between input and output voltages to prevent the power interface of being bypassed.
- Experimental validation using different generators.
- Implement and prototype a Current Controlled Boost Converter in a PCB.
- Mount the Signal Acquisition module in a PCB, to eliminate noise.
- Design and implement a power interface for commercial microinverters, up to 300 W.
- Design a new DC/DC converter topology, e.g., Buck-Boost Converter.

Bibliography

[1] V. Leite, J. Couto, Â. Ferreira, and J. Batista, "A practical approach for grid-connected pico-hydro systems using conventional photovoltaic inverters", in *2016 IEEE International Energy Conference (ENERGYCON)*, Apr. 2016, pp. 1–6. DOI: 10.1109/ENERGYCON.2016.7513911.

[2] United States Environmental Protection Agency, *Distributed Generation of Electricity and its Environmental Impacts*, [Online]. Available: https://www.epa.gov/energy/distributed-generation-electricity-and-its-environmental-impacts#main-content (visited on 08/20/2019).

[3] D. Harnesk and S. Brogaard, "Social dynamics of renewable energy—how the european union's renewable energy directive triggers land pressure in tanzania", *The Journal of Environment & Development*, vol. 26, no. 2, pp. 156–185, 2017. DOI: 10.1177/1070496516681043. [Online]. Available: https://doi.org/10.1177/1070496516681043.

[4] T. Ackermann, G. Andersson, and L. Söder, "Distributed generation: A definition1in addition to this paper, a working paper entitled 'distributed power generation in a deregulated market environment' is available. the aim of this working paper is to start a discussion regarding different aspects of distributed generation. this working paper can be obtained from one of the authors, thomas ackermann.1", *Electric Power Systems Research*, vol. 57, no. 3, pp. 195–204, 2001, ISSN: 0378-7796. DOI: https://doi.org/10.1016/S0378-7796(01)00101-8. [Online]. Available: http://www.sciencedirect.com/science/article/pii/S0378779601001018.

[5] C. Marnay, S. Chatzivasileiadis, C. Abbey, R. Iravani, G. Joos, P. Lombardi, P. Mancarella, and J. Von Appen, "Microgrid evolution roadmap", Sep. 2015, pp. 139–144. DOI: 10.1109/SEDST.2015.7315197.

[6] Berkeley Lab, *Microgrid Definitions*, [Online]. Available: https://building-microgrid.lbl.gov/microgrid-definitions (visited on 08/21/2019).

[7] S. Jain, S. Kalambe, G. Agnihotri, and A. Mishra, "Distributed generation deployment: State-of-the-art of distribution system planning in sustainable era", *Renewable and Sustainable Energy Reviews*, vol. 77, pp. 363–385, 2017, ISSN: 1364-0321. DOI: https://doi.org/10.1016/j.rser.2017.04.024. [Online]. Available: http://www.sciencedirect.com/science/article/pii/S1364032117305245.

[8] N. Acharya, P. Mahat, and N. Mithulananthan, "An analytical approach for dg allocation in primary distribution network", *International Journal of Electrical Power & Energy Systems*, vol. 28, no. 10, pp. 669–678, 2006, ISSN: 0142-0615. DOI: https://doi.org/10.1016/j.ijepes.2006.02.013. [Online]. Available: http://www.sciencedirect.com/science/article/pii/S0142061506000652.

[9] Eurostat, *Renewable energy statistics*, [Online]. Available: https://ec.europa.eu/eurostat/statistics-explained/index.php/Renewable_energy_statistics (visited on 08/24/2019).

[10] OFFICE of ENERGY EFFICIENCY & RENEWABLE ENERGY, *Project Profile: Evaluating the Causes of Photovoltaics Cost Reduction: Why is PV different?*, [Online]. Available: https://www.energy.gov/eere/solar/project-profile-evaluating-causes-photovoltaics-cost-reduction-why-pv-different (visited on 08/29/2019).

[11] A. Lahimer, M. Alghoul, K. Sopian, N. Amin, N. Asim, and M. Fadhel, "Research and development aspects of pico-hydro power", *Renewable and Sustainable Energy Reviews*, vol. 16, pp. 5861–5878, Oct. 2012. DOI: 10.1016/j.rser.2012.05.001.

[12] P. Bhusal, A. Zahnd, M. Eloholma, and L. Halonen, "Energy-efficient innovative lighting and energy supply solutions in developing countries", *International Review of Electrical Engineering (I.R.E.E.)*, vol. 2, Sep. 2007.

[13] J. Green, M. Fuentes, K. Rai, and S. Taylor, "Stimulating the picohydropower market for low-income households in ecuador", *Washington, D.C: Energy Sector Management Assistance Program (ESMAP)*, vol. 1, Dec. 2005.

[14] M. F. Basar, A. Ahmad, N. Hasim, and K. Sopian, "Introduction to the pico hydro power and the status of implementation in malaysia", in *2011 IEEE Student Conference on*

Research and Development, Dec. 2011, pp. 283–288. DOI: 10.1109/SCOReD.2011.6148751.

[15] R. Holland, L. Perera, T. Sanchez, and R. Wilkinson, "Decentralised rural electrification: Critical success factors and experiences of an ngo", *Refocus*, vol. 2, no. 6, pp. 28–31, 2001, ISSN: 1471-0846. DOI: https://doi.org/10.1016/S1471-0846(01)80060-3. [Online]. Available: http://www.sciencedirect.com/science/article/pii/S1471084601800603.

[16] G. S. Bruno, L. Fried, and D. Hopwood, "Focus on small hydro", *Renewable Energy Focus*, vol. 9, no. 6, pp. 54–57, 2008, ISSN: 1755-0084. DOI: https://doi.org/10.1016/S1755-0084(08)70068-1. [Online]. Available: http://www.sciencedirect.com/science/article/pii/S1755008408700681.

[17] T. N. Manders, J. I. Höffken, and E. B. van der Vleuten, "Small-scale hydropower in the netherlands: Problems and strategies of system builders", *Renewable and Sustainable Energy Reviews*, vol. 59, pp. 1493–1503, 2016, ISSN: 1364-0321. DOI: https://doi.org/10.1016/j.rser.2015.12.100. [Online]. Available: http://www.sciencedirect.com/science/article/pii/S1364032115014835.

[18] D. Gezer, Y. Taşcıoğlu, and K. Çelebioğlu, "Speed control of hydraulic turbines for grid synchronization using simple adaptive add-ons", *Measurement and Control*, vol. 51, p. 002 029 401 878 674, Jul. 2018. DOI: 10.1177/0020294018786743.

[19] J. Couto, "Exploitation of an interface for the connection to the grid of various distributed energy sources based on renewable energy", Master's thesis, Instituto Politécnico de Bragança, 2015, p. 76. [Online]. Available: http://hdl.handle.net/10198/12684 (visited on 02/10/2019).

[20] S. Kénio, "Plataforma para emulação de sistemas pico-hídricos ligados à rede elétrica, utilizando inversores fotovoltaicos convencionais", Master's thesis, Instituto Politécnico de Bragança, 2016, p. 76. [Online]. Available: http://hdl.handle.net/10198/14050 (visited on 03/10/2019).

[21] A. Fitzgerald, A. Fitzgerald, C. Kingsley, and S. Umans, *Electric Machinery*, ser. Electrical Engineering Series. McGraw-Hill Companies,Incorporated, 2003, ISBN: 9780073660097. [Online]. Available: https://books.google.pt/books?id=YBKk4kWSle0C.

[22] S. Chapman, *Electric Machinery Fundamentals*. McGraw-Hill Education, 2011, ISBN: 9780073529547. [Online]. Available: https://books.google.pt/books?id=L1TZtgAACAAJ.

[23] J. Gieras, *Electrical Machines: Fundamentals of Electromechanical Energy Conversion*. CRC Press, 2016, ISBN: 9781498708869. [Online]. Available: https://books.google.pt/books?id=6qWKDQAAQBAJ.

[24] J. Rocha, "Metodologia de projecto de sistemas de produção de electricidade descentralizada baseados em energia hídrica", Master's thesis, Universidade do porto, 2009, p. 212. [Online]. Available: http://hdl.handle.net/10216/60014 (visited on 08/31/2019).

[25] T. Wegiel and D. Borkowski, "Variable speed small hydropower plant", Jun. 2012, pp. 167–174, ISBN: 978-1-4673-2021-4. DOI: 10.1109/PEDG.2012.6253996.

[26] Power Spout, *Stators, Rotors & PMAs*, [Online]. Available: https://www.powerspout.com/collections/complete-smart-drive-pmas (visited on 07/23/2018).

[27] G. Harper, *El ABC De Las Maquinas Electricas / the ABC of Electrical Machines: Motores De Corriente Alterna/ Alternate Current Motors*, ser. El ABC de las máquinas eléctricas. Limusa, 2006, ISBN: 9789681826871. [Online]. Available: https://books.google.pt/books?id=m8xErTUnq7QC.

[28] "IEC 60196:2009", International Electrotechnical Commission, Geneva, CH, Standard, Jun. 2009.

[29] "IEEE Standard for Interconnection and Interoperability of Distributed Energy Resources with Associated Electric Power Systems Interfaces", *IEEE Std 1547-2018 (Revision of IEEE Std 1547-2003)*, pp. 1–138, Apr. 2018. DOI: 10.1109/IEEESTD.2018.8332112.

[30] *USER MANUAL OMNIKSOL*, Version 1.2, Omnik New Energy Co., Ltd., No.63, Wenxin Road, SIP, Suzhou, China, Jan. 2013.

[31] R. Teodorescu, M. Liserre, and P. Rodriguez, *Grid Converters for Photovoltaic and Wind Power Systems*, ser. Wiley - IEEE. Wiley, 2010, ISBN: 9780470667040.

[32] *Data Sheet - PIKO1.5-4-6 MP plus*, KOSTAL Solar Electric GmbH, Hanferstr. 6, 79108 Freiburg i. Br., Germany, Aug. 2018.

[33] *OPERATING MANUAL - SUNNY BOY 1300TL / 1600TL / 2100TL*, Version 1.1, SMA Solar Technology AG, Sonnenallee 1, 34266 Niestetal, Germany, 2014.

[34] *X1 SERIES USER MANUAL*, SolaX Power Co., LTD., No. 288 Shizhu Road, Tonglu Economic Development Zone, Tonglu City, Zheijian Province, China, Jun. 2019.

[35] A. C. Zamora, G. Vazquez, J. M. Sosa, P. R. Martinez-Rodriguez, and M. A. Juarez, "Efficiency based comparative analysis of selected classical mppt methods", in *2017 IEEE International Autumn Meeting on Power, Electronics and Computing (ROPEC)*, Nov. 2017, pp. 1–6. DOI: 10.1109/ROPEC.2017.8261657.

[36] A. Barchowsky, J. P. Parvin, G. F. Reed, M. J. Korytowski, and B. M. Grainger, "A comparative study of MPPT methods for distributed photovoltaic generation", in *2012 IEEE PES Innovative Smart Grid Technologies, ISGT 2012*, 2012, ISBN: 9781457721588. DOI: 10.1109/ISGT.2012.6175798.

[37] J.-A. Jiang, Y.-L. Su, K.-C. Kuo, C.-H. Wang, M.-S. Liao, J.-C. Wang, C.-K. Huang, C.-Y. Chou, C.-H. Lee, and J.-C. Shieh, "On a hybrid MPPT control scheme to improve energy harvesting performance of traditional two-stage inverters used in photovoltaic systems", *Renewable and Sustainable Energy Reviews*, vol. 69, pp. 1113–1128, 2017, ISSN: 1364-0321. DOI: https://doi.org/10.1016/j.rser.2016.09.112. [Online]. Available: http://www.sciencedirect.com/science/article/pii/S1364032116305986.

[38] A. Gaga, F. Errahimi, and N. Es-Sbai, "Design and implementation of MPPT solar system based on the enhanced P&O algorithm using Labview", in *2014 International Renewable and Sustainable Energy Conference (IRSEC)*, Oct. 2014, pp. 203–208. DOI: 10.1109/IRSEC.2014.7059786.

[39] V. Leite, Â. Ferreira, J. Couto, and J. Batista, "Compatibility analysis of grid-connected pico-hydro systems using conventional photovoltaic inverters", in *2016 18th European Conference on Power Electronics and Applications (EPE'16 ECCE Europe)*, Sep. 2016, pp. 1–9. DOI: 10.1109/EPE.2016.7695615.

[40] G. M. Ribeiro, W. Maidana, V. Leite, and A. Ferreira, "Grid connection approach for very small-scale pico-hydro systems using pv microinverters", (in press), 2019.

[41] Power Spout, *PowerSpout Document INDEX links*, [Online]. Available: https://docs.google.com/document/d/19O1bxXGqIjjsccm1onZj1X9Ae57ljK-rPLWEYzvZRN8/pub (visited on 11/21/2018).

[42] G. M. R. Isabella Cristina Scotta, W. Maidana, and V. Leite, "Over-Voltage Protection for Pico-Hydro Generation Using PV Microinverters", (Submitted), 2019.

[43] *TL494 Pulse-Width-Modulation Control Circuits*, Revision H, Texas Instruments, 12500 TI Boulevard Dallas, Texas 75243 USA, Jan. 2017.

[44] S. Samerchur, S. Premrudeepreechacharn, Y. Kumsuwun, and K. Higuchi, "Power control of single-phase voltage source inverter for grid-connected photovoltaic systems", in *2011 IEEE/PES Power Systems Conference and Exposition*, Mar. 2011, pp. 1–6. DOI: 10.1109/PSCE.2011.5772504.

[45] N. Mohan, T. Undeland, and W. Robbins, *Power electronics: converters, applications, and design*, ser. Power Electronics: Converters, Applications, and Design vol. 1. John Wiley & Sons, 2003, ISBN: 9780471226932.

[46] A. Ahmed, *Power Electronics For Technology*. PEARSON EDUCATION (US), 1998, ISBN: 9780132310697.

[47] S. Maniktala, *Switching Power Supplies A to Z*. Elsevier/Newnes, 2006, ISBN: 9780750679701. [Online]. Available: https://books.google.pt/books?id=VJTJEza9SMMC.

[48] R. D. Middlebrook and S. Cuk, "A general unified approach to modelling switching-converter power stages", in *1976 IEEE Power Electronics Specialists Conference*, Jun. 1976, pp. 18–34. DOI: 10.1109/PESC.1976.7072895.

[49] S. Maniktala, *Switching Power Supply Design & Optimization, Second Edition*, 2nd ed. New York: McGraw-Hill Education, 2014, ISBN: 9780071798143.

[50] N. Nise, *Control Systems Engineering, 7th Edition*. Wiley, 2015, ISBN: 9781118800829. [Online]. Available: https://books.google.pt/books?id=BwTYBgAAQBAJ.

[51] K. Ogata, *Modern Control Engineering*, ser. Instrumentation and controls series. Prentice Hall, 2010, ISBN: 9780136156734. [Online]. Available: https://books.google.pt/books?id=Wu5GpNAelzkC.

[52] Kiam Heong Ang, G. Chong, and Yun Li, "PID control system analysis, design, and technology", *IEEE Transactions on Control Systems Technology*, vol. 13, no. 4, pp. 559–576, Jul. 2005, ISSN: 1063-6536. DOI: 10.1109/TCST.2005.847331.

[53] *User's manual - ACS355 drives*, Rev D, ABB Ltd., Zurich, Switzerland, Jan. 2018.

[54] dSPACE, *ControlDesk*, [Online]. Available: https://www.dspace.com/en/pub/home/products/sw/experimentandvisualization/controldesk.cfm (visited on 08/27/2019).

[55] *Mitsubishi <Intelligent Power Modules> PM75RLA120 Flat-Base and Insulated Package Type*, Mitsubishi Electric Corporation, Tokyo Building, 2-7-3, Marunouchi, Chiyoda-ku, Tokyo 100-8310, Japan, May 2005. [Online]. Available: http://www.me-sh.cn/products/pdf/pm75rla120_e.pdf.

[56] *Powerex, BP7B –G1 Series Intelligent Power Module (IPM) Interface Circuit Reference Design*, Powerex Inc., 173 Pavilion Lane, Youngwood, PA 15697, USA, May 2005. [Online]. Available: www.pwrx.com/pwrx/docs/BP7B%20Application%20note.pdf.

[57] Matlab, *Find abrupt changes in data - MATLAB ischange*, [Online]. Available: https://www.mathworks.com/help/matlab/ref/ischange.html (visited on 07/20/2019).

Appendix A

Annexes

A.1 Codes

Listing A.1: Matlab script used to average the acquired data and exporting it

```
addpath('Test')
% Arrays for the avergaed values (scripture Optmization)
Ibmean   = zeros(4,12,4);
Vbmean   = zeros(4,12,4);
Pinmean  = zeros(4,12,4);
Idcmean  = zeros(4,300001,4);
Vdcmean  = zeros(4,300001,4);
% Poutmean = zeros(4,300001,4);
load('SB123.mat') % load addtional data for the SB 1000W
load('OMNIK014.mat') % load addtional data for the SB 1600W
%% saving the loaded data into the variables
Ib(4,:,1)   = [sb123.Y(1,3).Data];
Idc(4,:,1)  = [sb123.Y(1,5).Data];
Vb(4,:,1)   = [sb123.Y(1,8).Data];
Vdc(4,:,1)  = [sb123.Y(1,9).Data];
Pin(4,:,1)  = [sb123.Y(1,6).Data];
Pout(4,:,1) = [sb123.Y(1,7).Data];

Ib(1,:,4)   = [omnik014.Y(1,3).Data];
Idc(1,:,4)  = [omnik014.Y(1,4).Data];
```

```
Vb(1,:,4)   = [omnik014.Y(1,8).Data];
Vdc(1,:,4)  = [omnik014.Y(1,8).Data];
Pin(1,:,4)  = [omnik014.Y(1,5).Data];
Pout(1,:,4) = [omnik014.Y(1,6).Data];

nsample = 625; % number of samples used for averaging
%% scannig, averaging and exporting the data
for k=1:4 %k defines the Commercial PV inverter (from 1 to 4)
    for i=1:4 %i defines the test from 1 to 4
        if ((i==4) && (k==1))||(i==1) && (k==4)
            last = size(Ib,2); % defines matrix size for test 1
    with the Omniksol
        elseif (i==4) && (k==3)
            last=127500;                % defines matrix size
   for test 4 with the Solax
        elseif (i==2) && (k==4)
            last=148500;                % defines matrix size
   for test 2 with the Omniksol
        elseif (i==3) && (k==4)
            last=135000;                % defines matrix size
   for test 3 with the Omniksol
        elseif (i==4) && (k==4)
            last=160000;                % defines matrix size
   for test 4 with the Omniksol
        else
            last=149500;                % defines matrix size
   for every other
        end
```

```
43        [TFin,S1,S2] = ischange(Ib(i,1:last,k),'linear','
    MaxNumChanges',12); %analyze abrupt changes in value
44        [TFout,S3,S4] = ischange(Vdc(i,1:last,k),'linear','
    Threshold',200); %analyze abrupt changes in value
45        segline = S3.*t(1:last) + S4;
46        Tin     = find(TFin); % obtain the indices of the
    points in which changes happen
47        Tout    = Tin;  % Use same indices for output related
    data
48        indexin = [Tin-nsample last-nsample; Tin last];
49        indexout = [Tout-nsample last-nsample; Tout last];
50        for j=1:size(indexin,2) % obtain the mean values of Tin
    's nsample preceding samples
51            Ibmean(i,j,k)     = mean(Ib(i,indexin(1,j):indexin
    (2,j),k));
52            Vbmean(i,j,k)     = mean(Vb(i,indexin(1,j):indexin
    (2,j),k));
53            Pinmean(i,j,k)    = mean(Pin(i,indexin(1,j):indexin
    (2,j),k));
54        end
55        for m=1:size(indexout,2) % obtain the mean values of
    Tin's nsample preceding samples
56            Idcmean(i,m,k)    = mean(Idc(i,indexout(1,m):
    indexout(2,m),k));
57            Vdcmean(i,m,k)    = mean(Vdc(i,indexout(1,m):
    indexout(2,m),k));
58            Poutmean(i,m,k)   = mean(Pout(i,indexout(1,m):
    indexout(2,m),k));
59        end
```

```
60
61      end
62  end
63
64  %% Plot and Export the data
65  close all
66
67  for k=1:4
68      figure
69      subplot1 = subplot(1,2,1)
70      for i=1:4
71          plot(Vbmean(i,:,k),Ibmean(i,:,k),'LineWidth', 1.5)
72          hold on
73      end
74      xlabel('Voltage [V]')
75      ylabel('Current [A]')
76      grid on
77      legend('1.6 kW','1.3 kW','1.2 kW','1.0 kW','Location','NE')
78      title('Operation Zone at the Input')
79      set(gcf, 'Position', [0 0 2000 500]);
80      set(gcf, 'Color', 'w');
81      set(gca,'FontSize',16);
82      subplot2 = subplot(1,2,2)
83      for i=1:4
84          plot(Vdcmean(i,:,k),Idcmean(i,:,k),'LineWidth', 1.5)
85          hold on
86      end
87      xlabel('Voltage [V]')
88      ylabel('Current [A]')
```

```
    grid on
    legend('1.6 kW','1.3 kW','1.2 kW','1.0 kW','Location','NE')
    set(gcf, 'Position', [0 0 2000 500]);
    set(gcf, 'Color', 'w');
    set(gca,'FontSize',16);
    title('Operation Zone at the Output')
    if k==1
        xlim(subplot1,[100 300]);
        xlim(subplot2,[280 350]);
        export_fig('Results\SB\SB-2100TL-IV-mo.pdf');
    elseif k==2
        xlim(subplot1,[300 350]);
        xlim(subplot2,[300 350]);
        export_fig('Results\Kos\PIKO-IV-mo.pdf');
    elseif k==3
        xlim(subplot1,[250 400]);
        xlim(subplot2,[300 400]);
        export_fig('Results\Sol\Solax-IV-mo.pdf');
    elseif k==4
        xlim(subplot1,[300 400]);
        xlim(subplot2,[330 400]);
        export_fig('Results\Omn\Omniksol-IV-mo.pdf');
    end
    close
end
```

A.2 Raw data

The Voltage-Current curves shown in Figures A.1,A.2, ,A.3, and A.4 are the results of the plots using the raw data from all experimental tests.

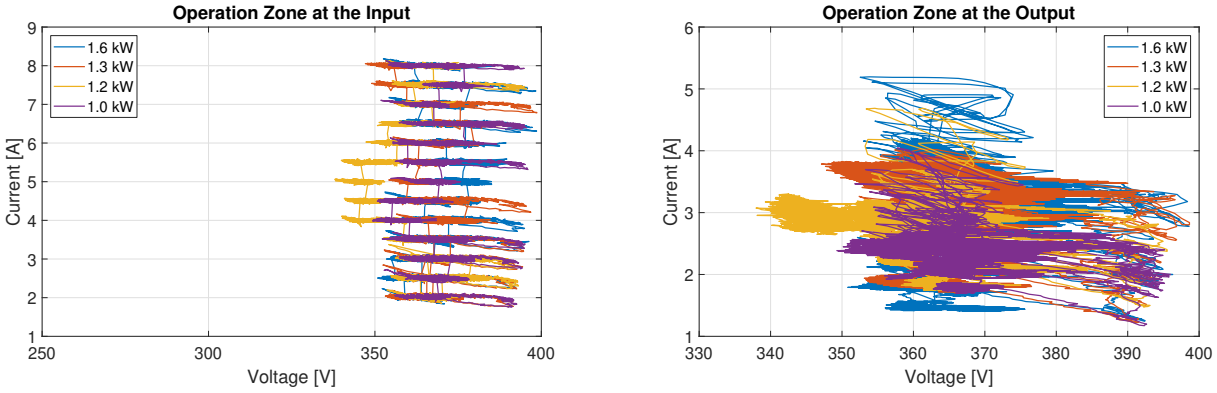

Figure A.1: Voltage-Current curve plotted withe the raw results from the four testes for Ominiksol-2k-TL2 CPVI.

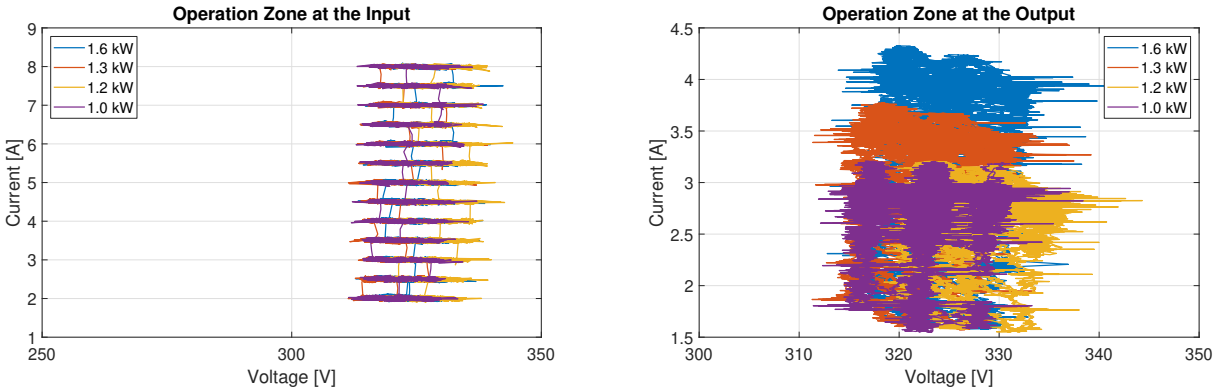

Figure A.2: Voltage-Current curve plotted withe the raw results from the four testes for Kostal Piko MP Plus CPVI.

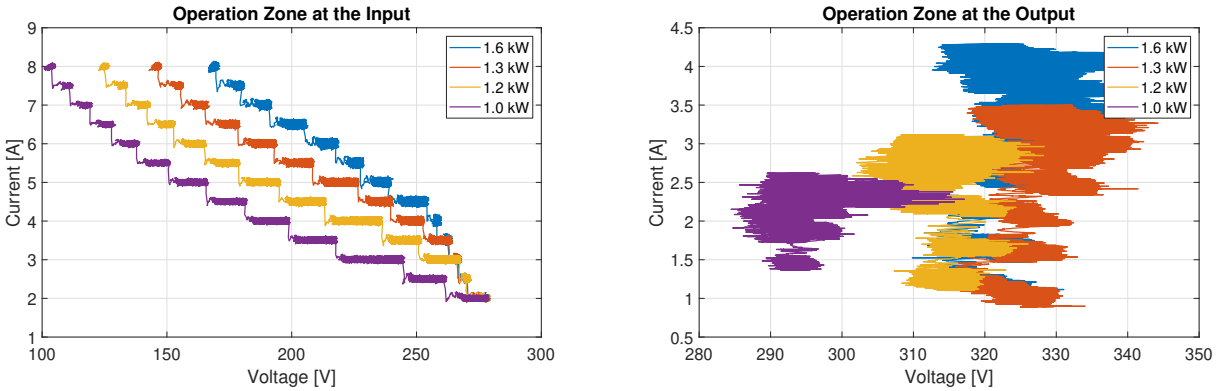

Figure A.3: Voltage-Current curve plotted withe the raw results from the four testes for SB 2100TL CPVI.

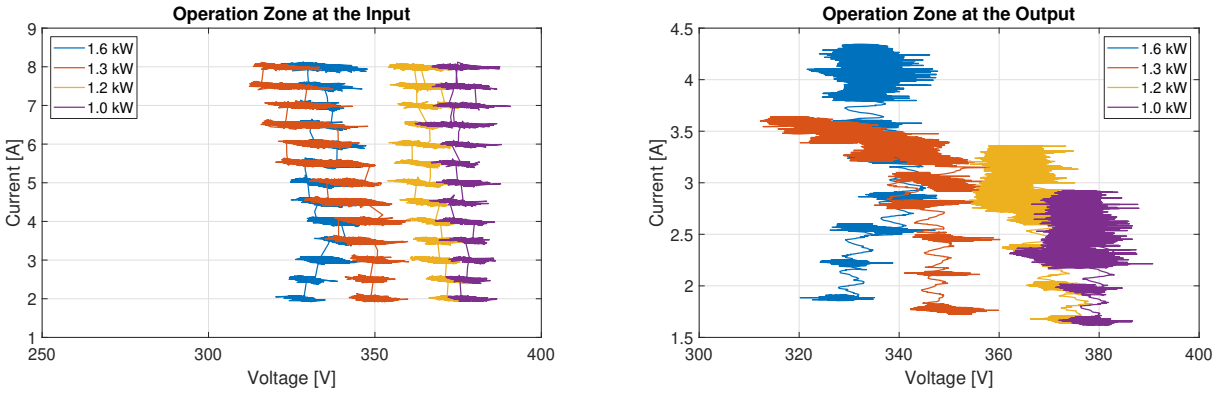

Figure A.4: Voltage-Current curve plotted withe the raw results from the four testes for Solax X1-1.5-S-D CPVI.